The Astronomical Journal, 156:302 (21pp), 2018 December https://doi.org/10.3847/1538-3881/aaeed7

Discovery of a Transiting Adolescent Sub-Neptune Exoplanet with *K2*

Trevor J. David[1], Eric E. Mamajek[1,2], Andrew Vanderburg[3,17], Joshua E. Schlieder[4], Makennah Bristow[5], Erik A. Petigura[6,18], David R. Ciardi[7], Ian J. M. Crossfield[8], Howard T. Isaacson[9], Ann Marie Cody[10], John R. Stauffer[11], Lynne A. Hillenbrand[6], Allyson Bieryla[12], David W. Latham[12], Benjamin J. Fulton[7], Luisa M. Rebull[11,13], Chas Beichman[14], Erica J. Gonzales[15,19], Lea A. Hirsch[9], Andrew W. Howard[6], Gautam Vasisht[1], and Marie Ygouf[16]
[1] Jet Propulsion Laboratory, California Institute of Technology, 4800 Oak Grove Drive, Pasadena, CA 91109, USA; trevor.j.david@jpl.nasa.gov
[2] Department of Physics & Astronomy, University of Rochester, Rochester, NY 14627, USA
[3] Department of Astronomy, The University of Texas at Austin, Austin, TX 78712, USA
[4] Exoplanets and Stellar Astrophysics Laboratory, Code 667, NASA Goddard Space Flight Center, Greenbelt, MD 20771, USA
[5] Department of Physics, University of North Carolina at Asheville, Asheville, NC 28804, USA
[6] Department of Astronomy, California Institute of Technology, Pasadena, CA 91125, USA
[7] Caltech/IPAC-NASA Exoplanet Science Institute, Pasadena, CA 91125, USA
[8] Department of Physics, Massachusetts Institute of Technology, Cambridge, MA, USA
[9] Astronomy Department, University of California, Berkeley, CA 94720, USA
[10] NASA Ames Research Center, Moffet Field, CA 94035, USA
[11] Spitzer Science Center (SSC), Infrared Processing and Analysis Center (IPAC), California Institute of Technology, Pasadena, CA 91125, USA
[12] Harvard-Smithsonian Center for Astrophysics, Cambridge, MA 02138, USA
[13] Infrared Science Archive (IRSA), Infrared Processing and Analysis Center (IPAC), California Institute of Technology, Pasadena, CA 91125, USA
[14] NASA Exoplanet Science Institute, California Institute of Technology, Jet Propulsion Laboratory, Pasadena, CA 91125, USA
[15] Astronomy and Astrophysics Department, University of California, Santa Cruz, CA, USA
[16] Infrared Processing and Analysis Center (IPAC), California Institute of Technology, Pasadena, CA 91125, USA
Received 2018 January 19; revised 2018 October 27; accepted 2018 November 4; published 2018 December 6

Abstract

The role of stellar age in the measured properties and occurrence rates of exoplanets is not well understood. This is in part due to a paucity of known young planets and the uncertainties in age-dating for most exoplanet host stars. Exoplanets with well-constrained ages, particularly those which are young, are useful as benchmarks for studies aiming to constrain the evolutionary timescales relevant for planets. Such timescales may concern orbital migration, gravitational contraction, or atmospheric photoevaporation, among other mechanisms. Here we report the discovery of an adolescent transiting sub-Neptune from *K2* photometry of the low-mass star EPIC 247267267. From multiple age indicators, we estimate the age of the star to be 120 Myr, with a 68% confidence interval of 100–760 Myr. The size of EPIC 247267267 b ($R_P = 2.8 \pm 0.1\ R_\oplus$) combined with its youth make it an intriguing case study for photoevaporation models, which predict enhanced atmospheric mass loss during early evolutionary stages.

Key words: open clusters and associations: individual (Cas-Tau) – planetary systems – planets and satellites: individual (EPIC 247267267 b) – planets and satellites: gaseous planets – planets and satellites: physical evolution – stars: low-mass

1. Introduction

Exoplanet properties are intrinsically linked to the properties of their host stars. The primary parameters governing stellar structure are mass, metallicity, and age. Planet occurrence is known to correlate with stellar mass (Cumming et al. 2008; Howard et al. 2012) and metallicity (Fischer & Valenti 2005). The degree to which planet demographics are time-dependent, however, remains underexplored. This is due to both the scarcity of known young planets as well as the large uncertainties in the ages of typical exoplanet hosts. Compiling a sample of planetary systems with well-constrained ages is a critical step on the path toward statistical comparisons of the frequencies and properties of planets across time.

There is a long history of planet searches within clusters and other coeval stellar populations. Early wide-field transit searches for hot Jupiters targeted globular clusters for the large sample sizes afforded by these populations (Gilliland et al. 2000; Weldrake et al. 2005, 2008). These searches resulted in no detections, leading to a claim of lower occurrence rates within older populations. However, Masuda & Winn (2017) revisited that claim and concluded the globular cluster null results were consistent with *Kepler* hot Jupiter statistics after accounting for frequency trends with stellar mass.

Within open clusters of intermediate (~1–7 Gyr) and young ages (<1 Gyr), numerous surveys have searched for planets across a wide range of mass and separation, using the transit, radial velocity (RV) and direct imaging methods (see Bowler 2016, for a review of young exoplanets detected through imaging). In the ~3.5 Gyr old M67 cluster, there is a claimed excess of hot Jupiters around solar-mass stars, while the rate of giant planets at wider separations seems to be in agreement with field statistics (Brucalassi et al. 2014, 2016, 2017). At intermediate ages, RV surveys searching for hot Jupiters in the nearby Hyades (~750 Myr) and Praesepe (~790 Myr) clusters have resulted in varying degrees of success (Cochran et al. 2002; Quinn et al. 2012, 2014). More recently, RV monitoring has revealed a number of hot Jupiters orbiting T Tauri and post–T Tauri stars (Donati et al. 2016; Johns-Krull et al. 2016; Yu et al. 2017).

As far as transit searches in clusters go, the majority of prior surveys were sensitive only to hot Jupiters yet still lacked the

[17] NASA Sagan Fellow.
[18] NASA Hubble Fellow.
[19] NSF Graduate Research Fellow.

combination of sensitivity and sample size needed to distinguish differences in planet populations in clusters and the field (see Janes & Kim 2009, for a review of early cluster surveys). A meta-analysis of early transit searches within open clusters showed that the null results from those surveys were consistent with expectations from field statistics (van Saders & Gaudi 2011). To date, only a single survey has compared the cluster and field occurrence rates of planets smaller than Neptune. That work used *Kepler* observations of the ∼1 Gyr old cluster NGC 6811 to find agreement between field and cluster rates, from two transiting planets around G-type stars (Meibom et al. 2013).

Compared with the *Kepler* mission, *K2* (Howell et al. 2014) has targeted a much more diverse set of astrophysical sources, enabling a wide range of Solar System, planetary, stellar, galactic, and extragalactic investigations. Since early 2014, *K2* has steadily assembled a legacy archive of precision photometry for more than 300,000 stars, including thousands of members of young clusters and associations. From these data, the first secure transiting planets in young (<1 Gyr) clusters have been established. For each of the clusters surveyed, the *K2* data are unprecedented in precision, cadence, baseline, and number of members surveyed. Recently, Rizzuto et al. (2017) presented a uniform search for transits in the *K2* cluster data. Our group is also involved in a parallel effort to measure the completeness of those data, laying the foundation for comparative planet occurrence at young ages.

A handful of the young transiting planets found with *K2* seem anomalously large compared to close-in planets around field-age stars of a similar mass, a possible hint for ongoing radius evolution (Mann et al. 2017a). However, most of the cluster planets transit low-mass (mid-K and later-type) stars, where our knowledge of planet populations is more incomplete relative to the solar-type (FGK) stars targeted by *Kepler*. Thus, the question that must be answered is whether these planets are large because they are young, or whether we are only finding them because they are easier to detect. An important step in answering this question is to compare the densities between young and old planets, but to date none of the known young exoplanets have both radius and mass measurements.

Close-in sub-Neptunes with ages $\lesssim$100 Myr are particularly interesting, given theoretical predictions that their cores may continue to be cooling (Vazan et al. 2017) and the atmospheres of such planets should experience enhanced photoevaporative mass loss at early times (Lopez & Fortney 2013; Owen & Wu 2013; Chen & Rogers 2016). The bimodal radius distribution of close-in sub-Neptunes has been interpreted as evidence of photoevaporative sculpting of this planet population (Fulton et al. 2017). Here we report the discovery and characterization of a sub-Neptune-sized planet transiting a young star ($\tau = 120^{+640}_{-20}$ Myr). The star's kinematics prior to *Gaia* DR2 were suggestive of membership with the poorly studied Cas-Tau association. However, the *Gaia* DR2 data weaken the case for membership and a detailed study of the existence, membership, and substructure of the association is left to a future work. Nevertheless, EPIC 247267267 b is one of the younger known transiting exoplanets and thus a useful benchmark for studying the evolution of close-in sub-Neptunes.

2. Observations

2.1. K2 Photometry

The *Kepler* space telescope observed EPIC 247267267 ($K_P = 12.811$ mag) between UT 2017 March 8 and 2017 May 27 during Campaign 13 of the *K2* mission. Due to roll angle variations and non-uniform intra-pixel sensitivity, photometry from the *K2* mission contains systematic artifacts, which are often much larger in amplitude than planet transit signals or even the intrinsic stellar variability. We corrected for these systematic effects using the K2SC package (Aigrain et al. 2016), which simultaneously models time- and position-dependent flux variations using Gaussian process regression. From these data, we discovered a periodic signal in a systematic search for transiting planets among the *K2* C13 targets (Figure 1). We also extracted photometry from a small square aperture (Figure 2) and circular apertures of different radii to mitigate the impact of nearby stars. The transits of EPIC 247267267 b are recovered at a consistent depth within apertures between 4″ and 16″ in radius. This argues against the transit signal being due to a diluted eclipsing binary (EB) at a projected separation larger than 4″. We also constructed a separate light curve, initially correcting for systematics using the K2SFF routine (Vanderburg & Johnson 2014), and then using that preliminary correction as a starting point to produce a light curve by performing a simultaneous least-squares minimization (prior to the transit model-fitting stage) to the transits, stellar activity, and systematics after removing flares (following Vanderburg et al. 2016). We flattened the light curve by dividing away the best-fit stellar variability pattern from the light curve. This light curve proved to be of higher precision, and we adopted it for the remaining analysis. From box-fitting least-squares periodogram analyses (Kovács et al. 2002) of light curves both including and excluding the transits of EPIC 247267267 b, we find no evidence for other periodic signals corresponding to additional transiting planets.

2.2. Literature Data

To aid our stellar characterization process, we gathered astrometric and photometric data from the literature. These data included a parallax, proper motions, and broadband photometry from *Gaia* DR2 (Gaia Collaboration et al. 2018b), as well as photometry from the *GALEX* DR5 (Martin et al. 2005), APASS DR9 (Henden et al. 2016), 2MASS (Cutri et al. 2003), and AllWISE (Cutri et al. 2013) catalogs. The photometric and astrometric properties of EPIC 247267267 are summarized in Table 1.

2.3. Adaptive Optics (AOs) Imaging

AOs imaging of EPIC 247267267 at K_s filter ($\lambda_\circ = 2.159$; $\Delta\lambda = 0.011$ μm) was acquired with the ShARCS infrared camera behind the ShaneAO AOs system on the Lick 3 m telescope on 2017 August 31 UT. The ShARCS camera has an unvignetted field of view approximately 20″ and has a pixel scale of 0.″033 pixel^{-1}. The AO data were obtained in a 9-point dither pattern with dither point separated by 5″ and a 60 s integration time per frame, for a total of 540 s. We used the dithered images to remove sky background and dark current, and then align, flat-field, and stack the individual images. The resolution of the Lick imaging was 0.″25 (FWHM), with a

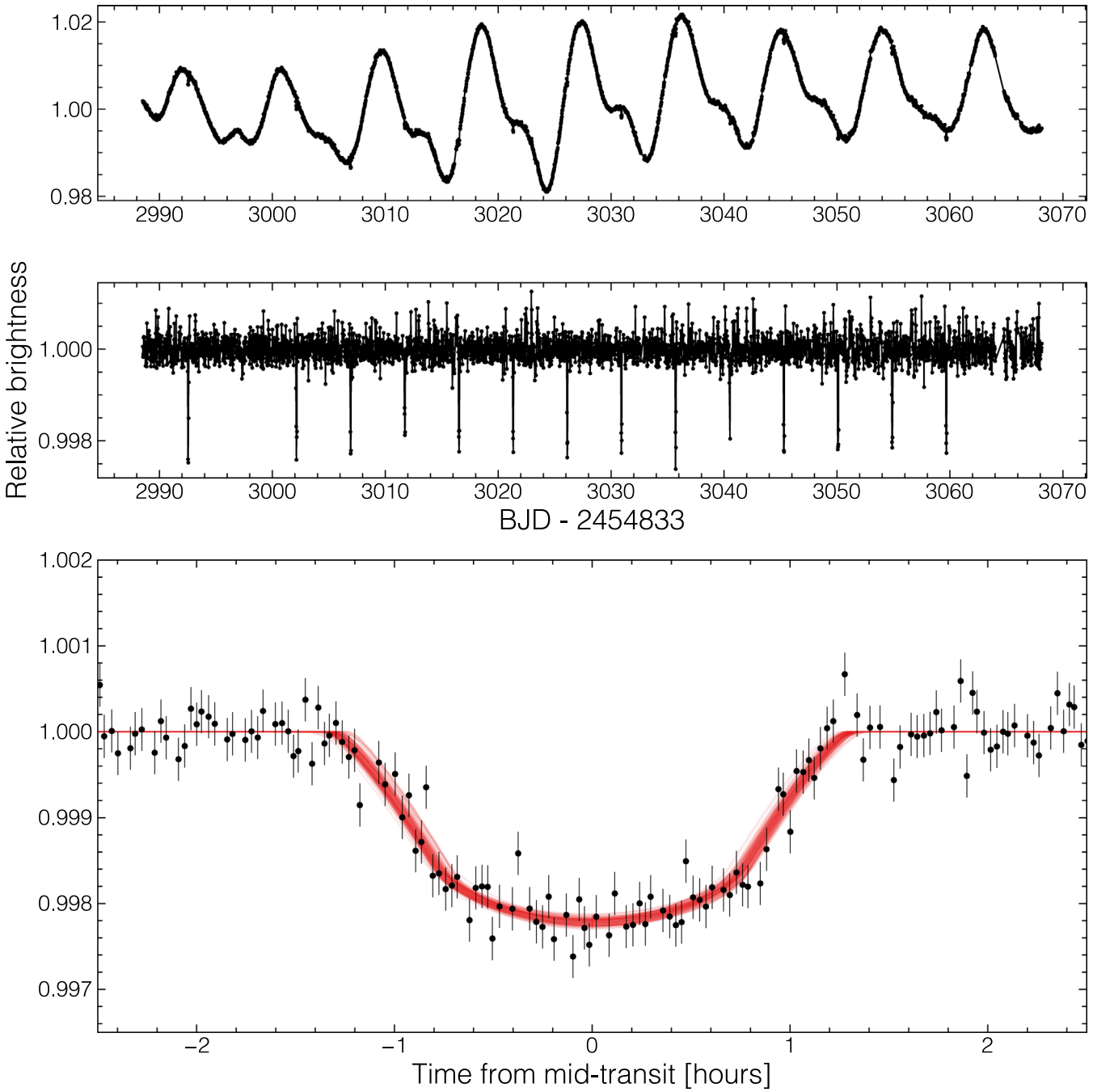

Figure 1. *K2* light curve of EPIC 247267267. In the top panel, the stellar variability pattern due to rotational modulation of starspots is apparent, as are the transits of EPIC 247267267 b. In the middle panel, the stellar variability has been removed. Missing transits are due to sections of the light curve that were removed in the detrending procedure. In the bottom panel, phase-folded model fits to the transits of EPIC 247267267 b. The red curves show 200 randomly selected models from the MCMC chain.

detection contrast of 2.8 mag at one FWHM separation from the target.

To obtain a higher resolution and deeper image, we also observed EPIC 247267267 with infrared high-resolution AOs imaging, both at Keck Observatory and Lick Observatory. The Keck Observatory observations were made with the NIRC2 instrument on Keck II behind the natural guide star AO system. The observations were made on 2017 October 31 in the narrow-band Br $-\gamma$ filter ($\lambda_o = 2.1686\,\mu$m, $\Delta\lambda = 0.0326\,\mu$m) in the standard 3-point dither pattern that is used with NIRC2 to avoid the left lower quadrant of the detector, which is typically noisier than the other three quadrants. The dither pattern step size was 3″ and was repeated three times, with each dither offset from the previous dither by 0.″5. The observations utilized an integration time of 10 s with one coadd per frame for a total of 90 s. The camera was in the narrow-angle mode with a full field of view of 10″ and a pixel scale of approximately 0.″1 per pixel. The resolution of the Keck imaging was 0.″06 (FWHM) with a detection contrast of 3.5 mag at one FWHM separation from the target.

The sensitivity of the final combined AO images was determined by injecting simulated sources separated from the primary target in integer multiples of the central source FWHM. The brightness of each injected source was scaled

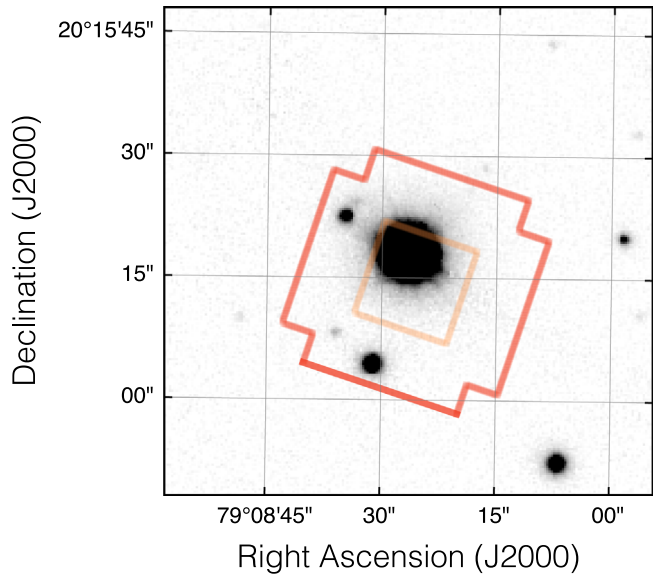

Figure 2. Pan-STARRS *r*-band image centered on EPIC 247267267 showing the adopted *K2* aperture in red and a smaller aperture in orange, from which the transits were also recovered at a consistent depth. We also inspected photometry from 4″ wide square apertures centered on the neighboring stars to the south and to the east to confirm that neither are eclipsing binaries.

Table 1
Astrometry and Photometry of EPIC 247267267

Parameter	Value	Source
Astrometry		
α R.A. (hh:mm:ss)	05:16:33.76	EPIC
δ Decl. (dd:mm:ss)	20:15:18.39	EPIC
μ_α (mas yr^{-1})	25.000 ± 0.082	*Gaia* DR2
μ_δ (mas yr^{-1})	−45.938 ± 0.059	*Gaia* DR2
ϖ (mas)	9.2935 ± 0.0431	*Gaia* DR2
Photometry		
NUV (mag)	21.688 ± 0.364	*GALEX* DR5
B (mag)	14.713 ± 0.006	APASS DR9
V (mag)	13.322 ± 0.015	APASS DR9
G (mag)	12.8598 ± 0.0011	*Gaia* DR2
g' (mag)	14.089 ± 0.034	APASS DR9
r' (mag)	12.758 ± 0.038	APASS DR9
i' (mag)	12.230 ± 0.011	APASS DR9
J (mag)	10.868 ± 0.024	2MASS
H (mag)	10.206 ± 0.025	2MASS
K_s (mag)	10.058 ± 0.018	2MASS
*W*1 (mag)	9.975 ± 0.023	AllWISE
*W*2 (mag)	10.007 ± 0.020	AllWISE
*W*3 (mag)	9.902 ± 0.060	AllWISE
*W*4 (mag)	>8.961	AllWISE

until standard aperture photometry detected the injected source with 5σ significance. The resulting brightness of the injected sources relative to the primary target set the 5σ contrast limits (see Figure 3). We find no evidence for nearby stars brighter than $\Delta K_s \approx 4$ mag outside of 0.″5, which corresponds to a K_p limit of ≈6 mag, using the $K_p - K_s$ empirical relation for dwarf stars (Howell et al. 2012), and is used to set the limits on the dilution of the observed transit (Ciardi et al. 2015) for the false-positive assessment (Section 3.2).

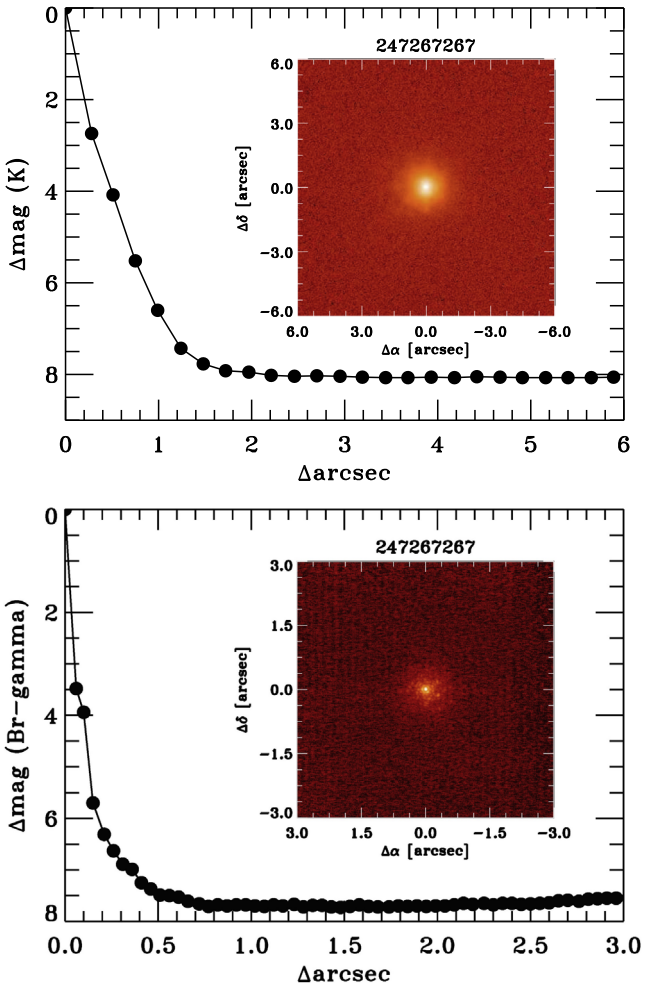

Figure 3. Contrast sensitivity and inset image of EPIC 247267267 in K_s, as observed with the Lick Observatory 3 m Shane adaptive optics system (above) and in Br-γ from the NIRC2 camera on the Keck II telescope (below). In each case, the 5σ contrast limit in Δ-magnitude is plotted against angular separation in arcseconds.

2.4. Keck I/HIRES

High-dispersion spectra of EPIC 247267267 were acquired on UT 2017 August 29 and November 8 using the HIRES spectrograph (Vogt et al. 1994) on the Keck I telescope. The spectra were obtained with the C2 decker, providing a spectral resolution of $R \approx 50{,}000$ in the range of ∼3640–7990 Å. The achieved SNR was 32/pixel at the peak of the blaze function near 5500 Å. The star's RV was measured from the HIRES spectra using the telluric A and B absorption bands as a wavelength reference (Chubak et al. 2012). These RVs are accurate at the ∼200 m s^{-1} level, which we adopt as the uncertainty on each telluric RV measurement. From the HIRES spectra, we also derived stellar parameters which we adopted for the remaining analysis. Our stellar characterization procedures are described in Section 3.4 and summarized in Table 4. The RV measurements from HIRES and Tillinghast Reflector Echelle Spectrograph (TRES; (described below) are reported in Table 2.

2.5. TRES

Using the TRES on the 1.5 m telescope at Fred L. Whipple Observatory, we observed EPIC 247267267 on UT

Table 2
Radial Velocities of EPIC 247267267

UT Date	BJD	RV (km s^{-1})	Instrument
2017 Aug 29	2457995.120599	16.85 ± 0.20	HIRES
2017 Sep 29	2458025.897972	17.23 ± 0.20	TRES
2017 Nov 8	2458066.060714	16.80 ± 0.20	HIRES

2017 September 29. The resolution of this spectrum is $R \approx$ 44,000 between 3850 and 9096 Å. From a 2600s integration, the achieved SNR is 18.9 per pixel at 5110 Å. We measured spectroscopic parameters and the absolute RV for EPIC 247267267 from the TRES spectrum using the Stellar Parameter Classification (SPC) tool (Buchhave et al. 2012, 2014). SPC measures RV from cross-correlating Kurucz (1992) synthetic template spectra with the target spectrum, allowing for rotational line broadening. We adopt an error of 0.2 km s^{-1} in the TRES RV, which is mainly due to the uncertainty in transforming the RV onto the IAU absolute velocity scale. The spectroscopic parameters found with SPC are broadly consistent with those found from the HIRES spectrum (see Section 3.4).

3. Analysis

3.1. Transit Model Fitting

We used the PYTRANSIT package (Parviainen 2015), based on the Mandel & Agol (2002) formalism, to generate transit models and fit these to the *K2* photometry. Parameter uncertainties were estimated through Markov chain Monte Carlo (MCMC) analysis using the EMCEE package (Foreman-Mackey et al. 2013). The free parameters in the transit fits are the orbital period ($P_{\rm orb}$), the time of mid-transit (T_0), the fractional stellar radius (R_*/a), the planet-star radius ratio (R_p/R_*), cosine of the inclination ($\cos i$), eccentricity (e), and the longitude of periastron (ω). We first performed a fit assuming a circular orbit, then relaxed this assumption and allowed eccentricity and the longitude of periastron to be free parameters. Transit models were numerically integrated to match the *Kepler* long cadence (1766 s) prior to fitting. For both fits, we initialized 50 walkers with 50,000 steps each. The autocorrelation length of each free parameter was estimated every 1000 steps, and once the chain length exceeded N times the autocorrelation length for each parameter and the fractional change in the autocorrelation length estimates was less than n %, the chain was considered to be converged and the MCMC sampler was halted. In the circular fit we used $N = 100$ and $n = 1\%$, while for the eccentric fit, we used $N = 50$ and $n = 2\%$. From the final chains, we determined the burn-in as 10 times the maximum autocorrelation length (1390 steps for the circular fit and 101,945 steps for the eccentric fit) and discarded these values. The median parameters of the transit fits determined from the truncated MCMC chains and the uncertainties, determined from the 16% and 84% quantiles, are reported in Table 3. For the eccentric fit, we assumed a Gaussian prior on the mean stellar density centered at 3.97 g cm^{-3} with width 0.47 g cm^{-3}. The mean stellar density prior originates from the stellar mass and radius we ultimately adopt, as described in Section 3.4. In both fits, we assumed quadratic limb-darkening parameters with Gaussian priors centered on $a_{\rm LD} = 0.7129$ and $b_{\rm LD} = 0.0229$ with widths of 0.11 and 0.036, respectively. The choice of limb-darkening values was based on our atmospheric parameters and interpolating between the tables of Claret et al. (2012). We found our model fitting, and hence overall conclusions, to be relatively insensitive to the precise choice of limb-darkening parameters. From the directly fitted parameters in the MCMC analysis, we derived the transit duration and mean stellar density using Equations (3) and (19) from Seager & Mallén-Ornelas (2003), respectively. The mean stellar density in the eccentric case was calculated from Equation (39) in Kipping (2010). The mean stellar density clearly indicates the planet is orbiting a dwarf star and not a giant, but we cannot rule out that the star is at the end of the pre-main-sequence phase of contraction. We note the equation for mean stellar density assumes a circular orbit, but the general conclusion remains unchanged, given the vast difference in stellar densities for dwarfs and giant stars. Transit model fits to the *K2* light curve are shown in Figure 1.

3.2. False-positive Assessment

Two nearby stars within 15″ of EPIC 247267267 are contained within our photometric aperture. The Pan-STARRS survey (Chambers et al. 2016; Flewelling et al. 2016) measured these sources, PSO J051634.085 + 201504.266 and PSO J051634.329 + 201522.312, to be approximately 4.42 mag and 5.52 mag fainter than EPIC 247267267 at r band, respectively. From Equation (7) of Ciardi et al. (2015), we calculated that the flux dilution from these nearby stars affects the inferred planet radius at a level of ≈1.2%, such that the true planet radius is negligibly larger than quoted. Here we are not concerned with this dilution, but with the possibility that this source or any other background source might be a contaminating EB that is being diluted by EPIC 247267267. The transit signature can be recovered with a consistent depth from photometry extracted using a 4″ radius aperture, though at lower signal-to-noise due to the difficulties of detrending in the face of increased aperture losses. This effectively argues against the possibility of the nearby star being a background EB, since its light should not contaminate the photometry extracted from the smaller aperture. Other nearby stars within 16″ either reside outside our aperture or are too faint to explain the observed transit depth (Figure 4).

In principle, an EB can dim by a maximum of 100% (although such systems are rare). The observed transit depth thus sets a limit on the faintness of a diluted EB of approximately $\Delta K_p \lesssim 6.9$ mag. In the simplified case of a target star with constant flux and a contaminating EB contained in the same photometric aperture, the observed depth of a diluted eclipse neglecting sky background is $\delta_{\rm obs} = \delta_{\rm ecl}\Delta F/(1 + \Delta F)$, where ΔF is the flux ratio between the target and the contaminating EB in the observed bandpass, and $\delta_{\rm ecl}$ is the intrinsic eclipse depth of the EB. In this case, if the nearby star is in fact an EB, only eclipses with depths greater than ≈28% depth are capable of producing the observed transit depth. We extracted photometry from small apertures centered on the neighboring stars to the south and to the east, finding no evidence for dimmings of a depth greater than the observed transit depth and at the period of EPIC 247267267 b. We have thus ruled out the possibility that either of the neighboring stars are EBs with periods comparable to the period of EPIC 247267267 b.

Using the TRILEGAL galactic model (Girardi et al. 2005), we simulated a 1-deg^2 field in the direction of EPIC 247267267. From the simulated field, we calculated the

Table 3
Results of EPIC 247267267 b Transit Fits

Parameter	Prior (Fit 1)	Value (Fit 1)	Prior (Fit 2)	Value (Fit 2)
Directly Sampled Parameters				
Orbital period, $P_{\rm orb}$ (days)	$\mathcal{U}(4.785, 4.805)$	$4.79507^{+0.00012}_{-0.00012}$	$\mathcal{U}(4.785, 4.805)$	$4.795069^{+0.000086}_{-0.000086}$
Time of mid-transit, T_0 (BJD-2450000)	$\mathcal{U}(7859.01726, 7859.20906)$	$7859.11316^{+0.00057}_{-0.00058}$	$\mathcal{U}(7859.01726, 7859.20906)$	$7859.11316^{+0.00043}_{-0.00042}$
Radius ratio, R_P/R_*	$\mathcal{U}(-1, 1)$	$0.0418^{+0.0011}_{-0.0010}$	$\mathcal{U}(-1, 1)$	$0.0420^{+0.0013}_{-0.0011}$
Scaled semimajor axis, a/R_*	$\mathcal{U}(0, \infty)$	$17.03^{+0.52}_{-0.66}$	$\mathcal{U}(0, \infty)$	$16.84^{+0.62}_{-0.70}$
Cosine of inclination, $\cos i$	$\mathcal{U}(\cos 90°, \cos 50°)$	$0.0166^{+0.0083}_{-0.0098}$	$\mathcal{U}(\cos 90°, \cos 50°)$	$0.017^{+0.011}_{-0.011}$
Eccentricity, e		0.0 (fixed)	$\mathcal{U}(0, 1)$	$0.078^{+0.108}_{-0.055}$
Longitude of periastron, ω (degrees)		0.0 (fixed)	$\mathcal{U}(0, 360)$	$180.2^{+126.4}_{-129.6}$
Limb-darkening coefficient, $a_{\rm LD}$	$\mathcal{G}(0.7129, 0.11)$	$0.697^{+0.093}_{-0.092}$	$\mathcal{G}(0.7129, 0.11)$	$0.684^{+0.094}_{-0.092}$
Limb-darkening coefficient, $b_{\rm LD}$	$\mathcal{G}(0.0229, 0.036)$	$0.034^{+0.030}_{-0.023}$	$\mathcal{G}(0.0229, 0.036)$	$0.034^{+0.031}_{-0.023}$
Derived Parameters				
Planet radius, R_P ($R_\oplus$)[a]	⋯	$2.77^{+0.12}_{-0.12}$	⋯	$2.78^{+0.14}_{-0.12}$
Semimajor axis, a (au)		$0.04771^{+0.00025}_{-0.00025}$		$0.04771^{+0.00025}_{-0.00025}$
Insolation flux, S ($S_\oplus$)	⋯	$42.6^{+1.8}_{-1.8}$	⋯	$42.6^{+1.8}_{-1.8}$
Equilibrium temperature, $T_{\rm eq}$ (K)[b]	⋯	649^{+15}_{-13}	⋯	653^{+16}_{-14}
Impact parameter, b	⋯	$0.28^{+0.13}_{-0.16}$	⋯	$0.28^{+0.19}_{-0.19}$
Inclination, i (degrees)	⋯	$89.05^{+0.56}_{-0.48}$	⋯	$89.00^{+0.65}_{-0.62}$
Total duration, T_{14} (hr)	⋯	$2.152^{+0.045}_{-0.043}$	⋯	$2.147^{+0.050}_{-0.045}$
Full duration, T_{23} (hr)	⋯	$1.963^{+0.050}_{-0.052}$	⋯	$1.950^{+0.051}_{-0.053}$
Mean stellar density, ρ_* (g cm^{-3})	$\mathcal{G}(3.97, 0.47)$	$4.06^{+0.39}_{-0.46}$	⋯	$3.91^{+1.07}_{-0.88}$

Note. $\mathcal{U}$: Uniform distribution (left bound, right bound). $\mathcal{G}$: Gaussian distribution (center, width). (a) The planet radius does not account for dilution from nearby stars within the photometric aperture, and may be negligibly larger by ≈1.2%. (b) The equilibrium temperature is calculated assuming an albedo of 0.3.

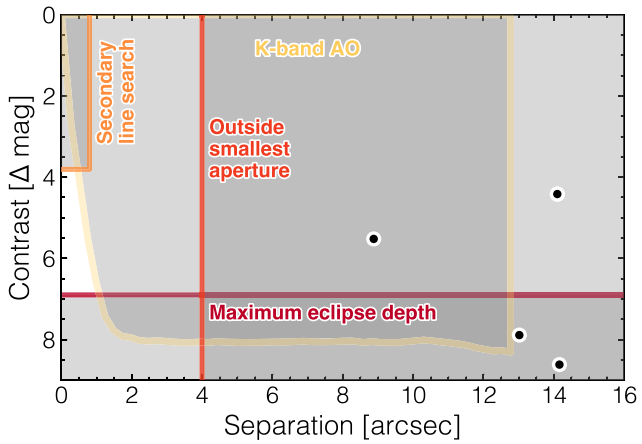

Figure 4. Contrast versus projected angular separation. The gray shaded regions show the excluded areas of parameter space in which a putative false positive could reside. The black points show nearby sources detected by Pan-STARRS. Note the secondary line search is blind to companions with velocity separations <15 km s^{-1} from the primary.

expected colors and surface density of background stars bright enough to produce the observed transit depth (i.e., $V \lesssim 20.2$ mag). We then scaled the resulting surface density by the size of the *K2* aperture to estimate the total number of expected contaminants. We found that <0.4 putative contaminants are expected within a 12″ aperture or <0.2 within an 8″ aperture. The number of expected contaminants that would be EBs is approximately two orders of magnitude smaller based on the statistical frequency of EBs in the *Kepler* field (Kirk et al. 2016). The mean near-IR colors of putative contaminants in the simulated field are $(J-H) = 0.49$ mag and $(H-K) = 0.08$ mag, suggestive of a K-type dwarf or giant. As noted earlier, the mean stellar density from the transit fit effectively rules out the possibility of a planet transiting a giant star.

We searched for secondary spectral lines in the HIRES spectrum from 2017 August 29 using the procedure described in Kolbl et al. (2015). We found no evidence for a nearby star down to 3% the brightness of the primary and within 0.″8. Notably, this method is blind to companions with velocity separations <15 km s^{-1}. We show the excluded regions of parameter space for hypothetical false-positive scenarios in Figure 4.

We also quantified the false-positive probability (FPP) using the `vespa` software package (Morton 2015). From the input *K2* photometry, the star's spectroscopic parameters and photometry, and high-resolution imaging constraints (the ShaneAO *K*-band contrast curve, in this case), `vespa` evaluated the relative likelihoods of transiting planet scenarios versus various diluted EB scenarios. The software accounts for binary population statistics and the ambient surface density of stars using the TRILEGAL galactic model. We found an overall FPP of 1/153, with the primary contributor to the FPP being an EB at twice the inferred period. In this case, one might expect differences in the depths of "odd" and "even" transits, so long as the hypothetical background EB has different primary and secondary eclipse depths.

As with any transiting planet candidate lacking a mass measurement, it is difficult to rule out all hypothetical false-positive scenarios. Nevertheless, from the qualitative arguments presented previously and the quantitative VESPA light curve analysis, we conclude that a transiting planet around EPIC 247267267 is the most secure interpretation for the *K2* signal.

3.3. Upper Limit to the Planet Mass

From three RV measurements, we find no evidence for orbital motion corresponding to Doppler semi-amplitudes

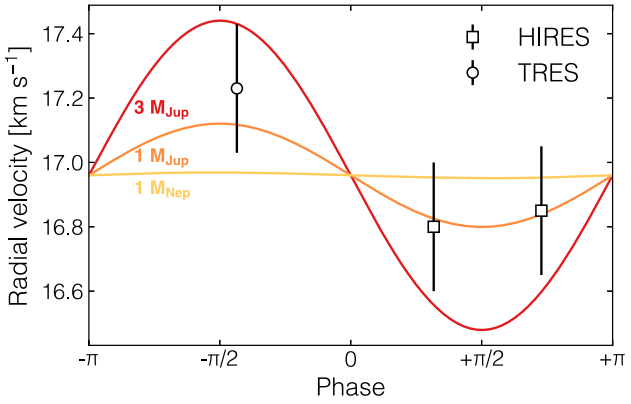

Figure 5. Radial velocities phased to the orbital ephemeris of EPIC 247267267 b. We find no evidence for orbital motion and from these measurements place an upper limit to the planet's mass of $<3\ M_{\rm Jup}$ at 95% confidence. The expected RV curves for planet masses corresponding to Neptune, Jupiter, and three times the mass of Jupiter are shown by the colored curves.

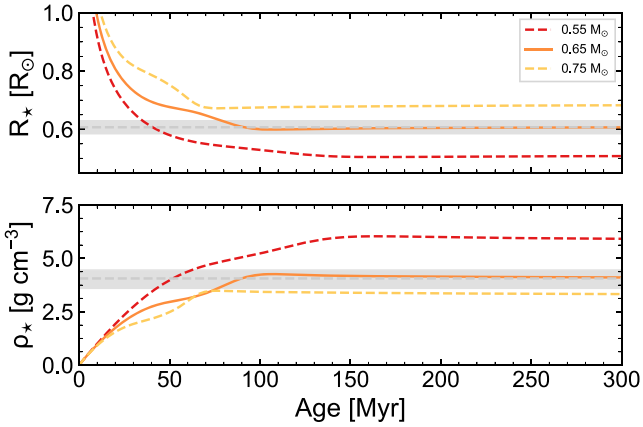

Figure 6. Theoretical predictions from the MIST models (Choi et al. 2016) of the evolution in radius (upper panel) and mean stellar density (lower panel) for low-mass stars. The gray lines and shaded regions show the adopted stellar radius and the mean stellar density measured from the transit fit.

greater than $\sim$200 m s^{-1} at the period of the planet (Figure 5). All three measurements are also consistent with being equal at the $\approx 1\sigma$ level. From these three measurements, we performed a one parameter MCMC fit to determine an upper limit to the Doppler semi-amplitude and thus the planet's mass. We performed these fits using the `radvel` package (Fulton et al. 2018),[20] fixing the planet's ephemeris to that determined from the transit fits and assuming a circular orbit. We did not allow for RV jitter, nor did we allow for any systematic offset between the HIRES and TRES RVs, as no such offset should exist. We fixed the systemic velocity to the value reported in Table 4. From this fit, we determined an upper limit to the mass of EPIC 247267267 b of $<3\ M_{\rm Jup}$ at 95% confidence, which rules out the possibility that a stellar or brown dwarf companion is responsible for the transits.

3.4. Stellar Characterization

Here we will discuss the various procedures used to characterize the host star. Unless otherwise noted, our quoted uncertainties in the non-spectroscopic parameters were derived through Monte Carlo simulations assuming normally distributed errors in the input parameters. Our spectroscopic analysis points to a dwarf-like gravity, suggesting that the star is on or very nearly on the ZAMS. The theoretical pre-main-sequence lifetime of a 0.65 $M_\odot$ star (corresponding to our adopted mass) is $\sim$110 Myr (see Figure 6). If EPIC 247267267 is in fact at the very end of its pre-main-sequence contraction, the true radius would still be encompassed by our radius uncertainties. Thus, our stellar characterization procedures are valid in employing spectral templates of field-aged stars, as well as empirical relations based on field star properties. The stellar parameters resulting from our characterization are reported in Table 4.

Spectroscopic characterization. From the HIRES spectrum, we determined the stellar $T_{\rm eff}$ (4108 ± 70 K), radius ($0.64 \pm 0.10\ R_\odot$), and [Fe/H] (-0.06 ± 0.09 dex) using the SpecMatch-Emp pipeline (Yee et al. 2017). SpecMatch-Emp uses a library of HIRES spectra for benchmark stars with securely measured parameters (via interferometry, asteroseismology, LTE spectral synthesis, and spectrophotometry) to find the optimal linear combination of these templates that matches a target spectrum. The parameters of the target star are determined via interpolation between the parameters for the templates in the optimal linear combination. The spectroscopic temperature and particularly the metallicity from the TRES spectrum and the SPC analysis ($T_{\rm eff,SPC} = 4288 \pm 50$ K, $_{\rm SPC} = -0.382 \pm 0.08$ dex) are in tension with the values found from SpecMatch-Emp. We do not have a satisfactory explanation for the metallicity discrepancy, but it may be related to the fact that the SpecMatch-Emp library of empirical

[20] https://github.com/California-Planet-Search/radvel

Table 4
Parameters of EPIC 247267267

Parameter	Value	Source
Kinematics and Position		
Barycentric RV (km s^{-1})	16.96 ± 0.19	HIRES, TRES
U (km s^{-1})	-14.5 ± 0.2	*Gaia* DR2 + RV
V (km s^{-1})	-27.6 ± 0.1	*Gaia* DR2 + RV
W (km s^{-1})	-5.56 ± 0.05	*Gaia* DR2 + RV
Distance (pc)	107.6 ± 0.5	*Gaia* DR2
Adopted Parameters		
M_* ($M_\odot$)	0.63 ± 0.01	isoclassify
R_* ($R_\odot$)	0.607 ± 0.022	isoclassify
L_* ($L_\odot$)	0.097 ± 0.004	isoclassify
$T_{\rm eff}$ (K)	4140 ± 50	isoclassify
log g (dex)	4.67 ± 0.01	isoclassify
[Fe/H] (dex)	0.00 ± 0.08	isoclassify
A_V (mag)	0.27 ± 0.05	$T_{\rm eff}$, $B-V$, PM13
Rotation period (days)	8.88 ± 0.40	*K2*
$v \sin i_*$ (km s^{-1})	3.54 ± 0.50	TRES+SPC
log R'_{HK} (dex)	-3.9 ± 0.5	HIRES
S-index	5 ± 1	HIRES
Estimated Age		
$\tau_{\rm isoc,1}$ (Myr)	113^{+703}_{-25}	$T_{\rm eff}$, L_*
$\tau_{\rm isoc,2}$ (Myr)	133^{+573}_{-69}	$T_{\rm eff}$, ρ_*
$\tau_{\rm gyro,1}$ (Myr)	124^{+13}_{-15}	$P_{\rm rot}$, $(B-V)_0$, B07
$\tau_{\rm gyro,2}$ (Myr)	262^{+35}_{-41}	$P_{\rm rot}$, $(B-V)_0$, MH08
$\tau_{R'_{HK}}$ (Myr)	139^{+1353}_{-119}	log R'_{HK}, MH08
$\tau_{\rm NUV}$ (Myr)	111^{+160}_{-65}	$(\mathrm{NUV}-J)_0$, $(J-K)_0$, F11
τ_* (Myr)	120^{+640}_{-20}	

Note. PM13: Pecaut and Mamajek (2013), B12: Boyajian et al. (2012), M15: Mann et al. (2015), B07: Barnes (2007), MH08: Mamajek and Hillenbrand (2008), F11: Findeisen et al. (2011).

template stars in this temperature range do not sample an evenly spaced range of metallicities. Notably, the effective temperature inferred from the star's photometric colors and empirical relations (Pecaut & Mamajek 2013; Mann et al. 2015) is closer to the value from the SpecMatch-Emp analysis.

Spectral type and extinction. The best-matching template star from the SpecMatch-Emp analysis is GJ 3494, which has been assigned spectral types of M0 and K5 (Skiff 2014). From the spectroscopically determined $T_{\rm eff}$ and the empirical spectral-type-$T_{\rm eff}$ relations presented in Pecaut & Mamajek (2013), hereafter PM13, we find the $T_{\rm eff}$ to be consistent with a spectral type of K6.5. Given the stellar effective temperature, we interpolated between the empirical $T_{\rm eff}$-$(B-V)_0$ relation of PM13 to determine an expected intrinsic color of $(B-V)_0 = 1.305$ mag, corresponding to a color excess of $E(B-V) = 0.086 \pm 0.016$ mag. We then assumed the Cardelli et al. (1989) extinction curve to derive A_V. We used the $(B-V)$ color excess noted previously and the extinction coefficients derived by Yuan et al. (2013) for the *GALEX* and 2MASS passbands to derive near-UV and near-IR colors, which we later use to estimate the stellar age, as described in Section 3.5.

Mass, radius, and luminosity. We derived the luminosity using the spectroscopically determined $T_{\rm eff}$, radius and the Stefan-Boltzmann law. We derived a separate luminosity estimate from an empirical $T_{\rm eff}$-luminosity relation based on interferometry of low-mass stars (Boyajian et al. 2012). This second estimate is not entirely independent of the first estimate, since the spectroscopic parameter pipeline is calibrated to the same interferometric standards, among other benchmark stars. We derived a model-dependent mass from a theoretical H-R diagram using the solar-metallicity ($Z = 0.0152$) PARSECv1.2S models (Bressan et al. 2012; Chen et al. 2014), our spectroscopically determined $T_{\rm eff}$, and the Stefan-Boltzmann determined luminosity. We also derived a distance-dependent mass from the kinematic distance, the apparent K_s magnitude, and a semi-empirical mass-M_{K_s} relation (Mann et al. 2015). Notably, this mass is 2σ lower than the model-dependent mass we adopt. We assume the discrepancy is due to the uncertainty in the distance. If the mass estimate from this empirical relation is correct, the mean stellar density from the transit fit would seem to reinforce the notion that the star is still on the pre-main-sequence. However, as a sanity check we compared our stellar parameters with those of the nearly equal-mass benchmark EB GU Boo (López-Morales & Ribas 2005), which agree reasonably well with our adopted mass, radius, and temperature.

We used the `isoclassify`[21] package (Huber et al. 2017) in Python for our final determination of the stellar mass, radius, and luminosity. The package has two operational modes, both of which take input observables (in our case, spectroscopic constraints, photometry, and parallax) in order to derive stellar parameters. In the "grid" mode, `isoclassify` takes the input observables and interpolates between the MIST isochrones (Choi et al. 2016; Dotter 2016) to derive posterior probability densities for $T_{\rm eff}$, $\log g$, [Fe/H], R_*, M_*, ρ_*, L_*, age, distance, and A_V. In the "direct" mode, the software can take the same input parameters and use bolometric corrections (taken from the MIST models) and extinction maps to determine $T_{\rm eff}$, R_*, L_*, distance, and A_V directly from physical relations. We classified EPIC 247267267 in both modes using the HIRES spectroscopic $T_{\rm eff}$ and [Fe/H] constraints, the $\log g$ constraint from TRES, the *Gaia* DR2 parallax, and *JHK*+*gri* photometry. Both modes predicted stellar radii that were consistent within 1σ, and we ultimately adopted the mass, radius, and luminosity from the grid method, though with the more conservative radius uncertainties derived from the direct method. We also checked that the parameters did not change substantially when only including the *JHK* photometry or only the *K* magnitude.

[21] https://github.com/danxhuber/isoclassify

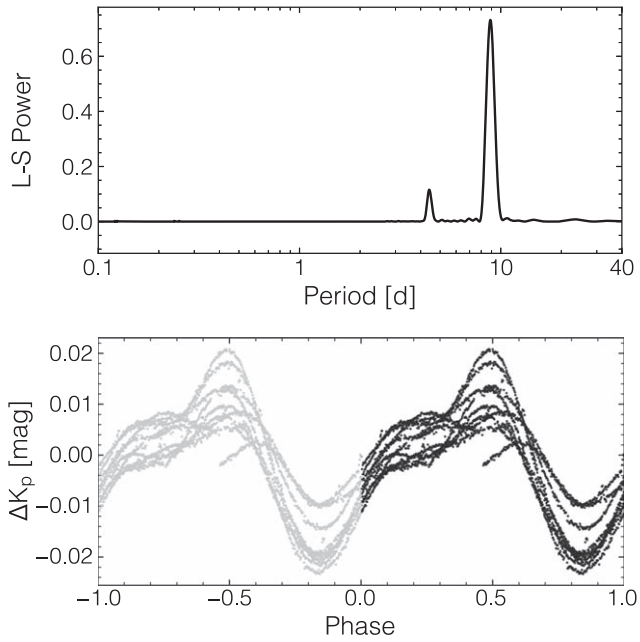

Figure 7. Lomb–Scargle periodogram from *K2* photometry of EPIC 247267267 (top) and the light curve phased to the rotation period of 8.88 days (bottom).

Rotation period and projected rotational velocity. A period of 8.88 ± 0.40 days, which we attribute to surface rotation of the star, was measured from a Lomb–Scargle periodogram analysis (Lomb 1976; Scargle 1982) of the *K2* light curve (Figure 7). The uncertainty in the rotation period was estimated from the standard deviation of a Gaussian fit to the oversampled periodogram peak. This uncertainty is likely overestimated, but encompasses the more difficult to quantify uncertainty in the rotation period due to, for example, differential rotation. The formal uncertainty, estimated by the periodogram peak width divided by the peak signal-to-noise, is 0.0085 days. A second peak in the periodogram at 4.41 ± 0.11 days is a harmonic of the true rotation period. The projected rotational velocity, $v_* \sin i_* = 3.54 \pm 0.50$ km s^{-1}, was measured from the TRES spectrum by broadening synthetic template spectra to match the observations. An independent and consistent $v_* \sin i_*$ estimate of 3–4 km s^{-1} was found from the HIRES spectrum and SpecMatch-Emp by broadening empirical template spectra, assuming the template stars were not rotating. Using the TRES value and the *K2* rotation period, we estimated the minimum stellar radius, $R_* \sin i_* = 0.621 \pm 0.092$ $R_\odot$. This value is within the uncertainty of our adopted radius, suggesting the stellar spin-axis is nearly edge-on. Put another way, for our adopted radius, the measured photometric rotation period, and assuming a uniform distribution in $\cos i_*$, the median and 68% confidence interval predicted for $v_* \sin i_*$ is 3.6 ± 0.6 km s^{-1}, in good agreement with our measurements.

Kinematics, Membership, and Distance. The EPIC catalog contains a preliminary photometric distance estimate of 84^{+18}_{-11} pc, assuming the star is on the main sequence (Huber et al. 2016). *Are there any nearby young stellar populations that EPIC 247267267* might be a kinematic member of which could help in constraining its age? EPIC 247267267 occupies a busy region of sky with regard to nearby young stellar populations. Within 200 pc and within 30° of EPIC 247267267's position are three open clusters (Hyades, 32 Ori & Pleiades): the Tau-Aur association, the Cas-Tau association, and the recently identified 118 Tau group. The *Gaia* DR2 proper motions for EPIC 247267267 are μ_α, $\mu_\delta = 25.000$, -45.938 ($\pm 0.082, \pm 0.059$) mas yr^{-1}. The proper motions were compared to the proper motions and radial velocities of members of these groups from the literature. EPIC 247267267's proper motion is clearly inconsistent with the nearby 118 Tau group (μ_α, $\mu_\delta = 4$, -39 mas yr^{-1}). Although EPIC 247267267's RV (16.96 ± 0.19 km s^{-1}) is similar to that of the Tau-Aur association ($+16$ km s^{-1}, Luhman et al. 2009), its proper motion is very different compared to the mean proper motion for the group (μ_α, $\mu_\delta = 6$, -21 mas yr^{-1}), or any of the subgroups (Luhman et al. 2009).

The only group that provides a near match of proper motion and RV is the Cas-Tau association. Prior to the determination of a parallax from *Gaia* DR2, we used the methodology of Mamajek (2005), the UCAC5 (Zacharias et al. 2017) proper motion for EPIC 247267267, and the "spaghetti" velocity solution from de Zeeuw et al. (1999), to find the bulk of EPIC 247267267's proper motion appeared to be moving toward the Cas-Tau convergent point ($\mu_v = 51.3 \pm 1.2$ mas yr^{-1}) with negligible perpendicular motion ($\mu_\tau = 4.7 \pm 1.2$ mas yr^{-1}). The predicted kinematic distance from this analysis was 79 ± 10 pc (kinematic parallax $\varpi = 12.7 \pm 1.6$ mas), with predicted RV $v_r = 15.4$ km s^{-1} (compared to our measured value of 16.96 ± 0.19 km s^{-1}), and predicted peculiar motion 1.7 ± 0.5 km s^{-1}. However, contradicting the spaghetti velocity solution, the true distance to the system now provided by *Gaia* DR2 is $d = 107.6 \pm 0.5$ pc.

De Zeeuw et al. (1999) estimated the space velocity of Cas-Tau using the spaghetti method with their *Hipparcos* membership to be U, V, $W = -13.24$, -19.69, -6.38 km s^{-1} (U positive toward the galactic center). As a check, and to provide a modern estimate, we cross-referenced de Zeeuw's membership of Cas-Tau members with the revised *Hipparcos* catalog (van Leeuwen 2007), *Gaia* DR1 (preferred, when available), and the RV compilation of Gontcharov (2006). This provided UVW velocity estimates for 48 candidate Cas-Tau members. These are plotted in Figure 8, along with the mean velocities for the Cas-Tau group from de Zeeuw et al. (1999), and the α Persei cluster, along with the values for EPIC 247267267 given by the *Gaia* DR2 kinematics and the RV we determined here. The median *UVW* for the 48 members is U, V, $W = -14.7 \pm 0.9$, -21.3 ± 0.8, -7.1 ± 0.4 km s^{-1}. Using the probit method, which is resilient to the effects of extreme values, the 1σ scatters reflecting the core of the velocity distributions are estimated as 3.9, 3.7, 2.7 km s^{-1}. Accounting for the mean *UVW* velocity component uncertainties (2.4, 1.9, 1.4 km s^{-1}), this suggests the intrinsic U, V, W velocity dispersions among the de Zeeuw et al. Cas-Tau membership to be approximately 3.0, 3.1, and 2.2 km s^{-1}. This likely reflects the adopted 3 km s^{-1} velocity dispersion used by de Zeeuw et al. in their original kinematic membership selection. Further work is needed to clarify the membership of Cas-Tau with *Gaia* astrometry, and to search for kinematic and age substructure; however, this is beyond the scope of this study. In Appendix, we discuss the history of the Cas-Tau association, examine the main-sequence turnoff for proposed members, and derive a new estimate of the association age.

We also used the BANYAN Σ tool (Gagné et al. 2018) to estimate the membership probability of EPIC 247267267 to various young moving groups and clusters within 150 pc. We note that the proposed Cas-Tau association is not included in BANYAN. We calculated membership probabilities both including and excluding the XYZ position of the star. The latter scenario is useful for identifying putative moving group or cluster members that are widely separated on the sky from the core population. The closest kinematic match among the young associations included in BANYAN was Tau-Aur, although the most likely hypothesis found in both cases is that EPIC 247267267 is a field star with 99.9% probability.

3.5. Youth Indicators

Rotation: The photometric rotation period provides evidence of youth, as shown in Figure 9. For a star of its mass or color, EPIC 247267267 has a rotation period consistent with the slowly rotating sequence of Pleiades members (Rebull et al. 2016), but about 3–4 days shorter than expected for members of Praesepe (Rebull et al. 2017) or the Hyades (Douglas et al. 2016). Given the star's intrinsic $(B-V)$ color and its rotation period, we calculated the age of the star using the gyrochronology relations of both Barnes (2007), hereafter B07, and Mamajek & Hillenbrand (2008), hereafter MH08. Our gyrochronology ages take into account the uncertainties in the rotation period, $(B-V)$ color, as well as the published errors on the coefficients in the age-rotation relations (see Table 4). The B07 calibration produces an age that is roughly a factor of two younger than the age predicted from the MH08 relations ($\tau_{\rm gyro,MH08} = 124$ Myr, compared to $\tau_{\rm gyro,MH08} = 262$ Myr). For completeness, we also investigated the Angus et al. (2015), hereafter A15, gyrochronology calibration and found that it closely reflects the MH08 predictions in the age and color range of interest here. To further investigate the differences and potential systematics in existing gyrochronology calibrations, we compared the relations to the intrinsic $(B-V)$ colors and rotation periods for members of the Pleiades and Praesepe clusters. The Pleiades photometry was gathered from Stauffer & Hartmann (1987) and Kamai et al. (2014); the Praesepe photometry was gathered from Upgren et al. (1979), Weis (1981), Stauffer (1982), and Mermilliod et al. (1990); and the rotation periods originate from Rebull et al. (2016, 2017). For this exercise, we assumed $E(B-V) = 0.04$ for the Pleiades, and no reddening for Praesepe. Figure 9 shows that the B07 calibration most closely matches the Pleiades's slowly rotating sequence at the accepted age of the cluster, while the MH08 and A15 relations overpredict the age of the Pleiades. It is worth noting that all existing gyrochronology calibrations predict a younger age for Praesepe (∼500–600 Myr) that is more in line with recent color–magnitude diagram (CMD) estimates (Gossage et al. 2018), but in tension with the older estimate of ∼790 Myr from Brandt & Huang (2015). A complete reassessment of gyrochronology calibrations using the voluminous rotation data now provided by *K2* is in order but outside the scope of this paper. We tentatively conclude that the younger

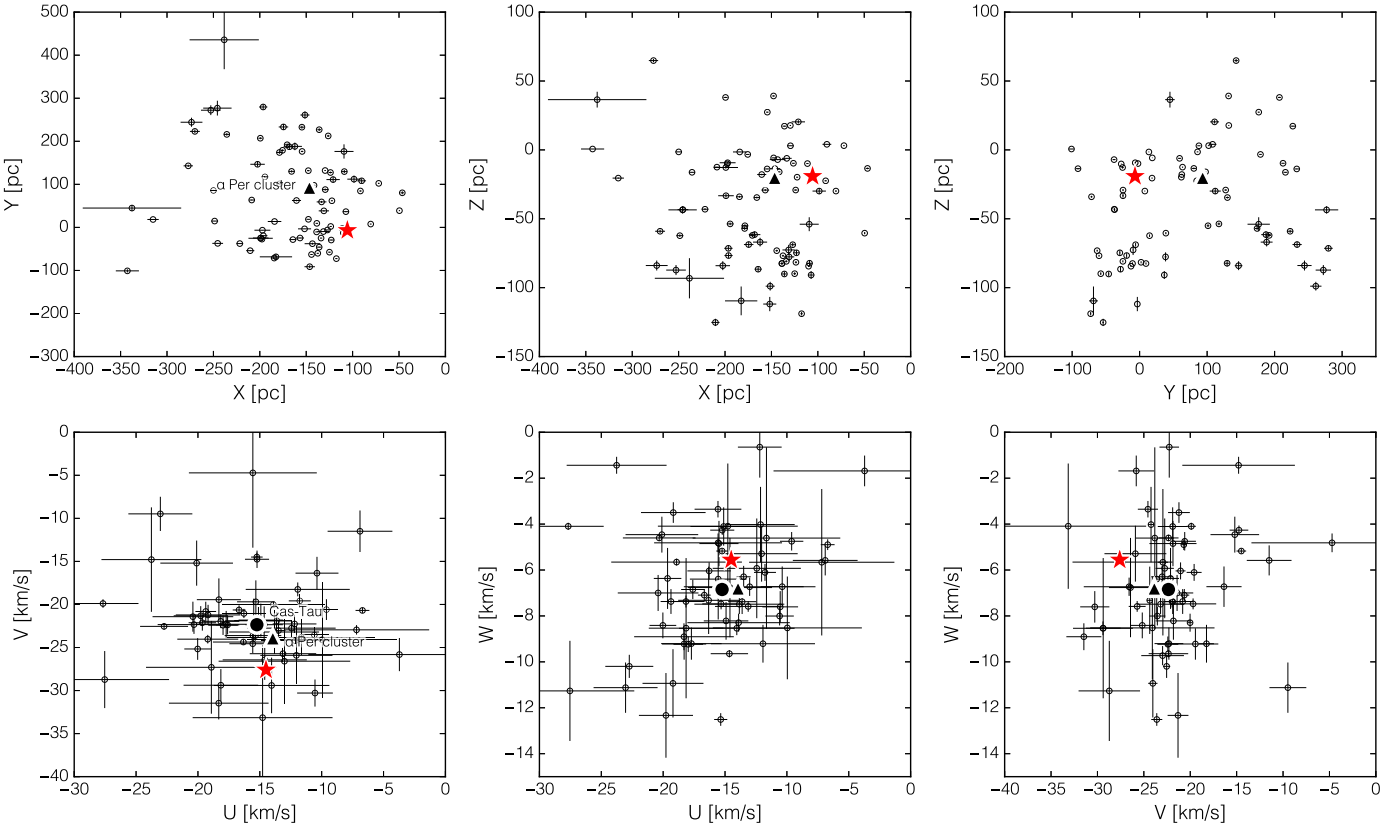

Figure 8. XYZ positions and UVW space motions for proposed Cas-Tau members (open circles; de Zeeuw et al. 1999), the α Per cluster (filled triangle; based on the *Gaia* DR2 astrometry and radial velocity from Gaia Collaboration et al. 2018a), and EPIC 247267267 (red star). The error bars reflect 1σ uncertainties for de Zeeuw et al. (1999) Cas-Tau members using *Gaia* DR2 parallaxes, combined with RVs from DR2, when available, or de Bruijne and Eilers (2012) otherwise. In the bottom panels, the filled circle indicates the median velocity of the proposed Cas-Tau members, without outlier rejection. The cluster of points in the lower right of the first two panels is due to the newly identified μ Tau group, which will be the subject of a future work.

gyrochronology age of EPIC 247267267 predicted by the B07 relations is likely to be more accurate, given the ability of that calibration to reproduce the Pleiades data, but also note that gyrochronology is fundamentally a statistical age-dating method, only applicable to main-sequence stars, and assumes the star is on the slowly rotating sequence. In this case, our stellar characterization suggests EPIC 247267267 has indeed arrived on the main sequence, and other youth indicators discussed as follows are consistent with an age similar to that of the Pleiades.

Chromospheric activity: EPIC 247267267 shows significant emission in the Ca II H&K lines (Figure 10). The precise H&K values in our spectra are ambiguous due to the low SNR of ~4 per pixel in the H&K orders. Nevertheless, we report our measured $\log R'_{HK}$ and the S-index with large uncertainties in Table 4. Our best estimate of $\log R'_{HK}$ is just barely outside the high-activity range where the activity-age relations of Mamajek & Hillenbrand (2008) were calibrated. Regardless, we estimated an activity age by modeling $\log R'_{HK}$ as a normal distribution with the values specified in Table 4 and imposing a cutoff upward of −4.0. From this analysis, we estimated the activity age to be <435 Myr at 68% confidence.

Near-UV emission: While there is no X-ray detection of EPIC 247267267, the star was detected at near-UV wavelengths with *GALEX*. Young, low-mass stars have been shown to exhibit significant emission above photospheric levels in the near-UV (NUV, 1750–2750 Å) and far-UV (FUV, 1350–1750 Å) *GALEX* passbands (Findeisen & Hillenbrand 2010; Rodriguez et al. 2011, 2013; Shkolnik et al. 2011; Kraus et al. 2014). Specifically, Shkolnik et al. (2011) found that young (<300 Myr) late-K and M-dwarfs generally show fractional flux densities of $F_{\rm NUV}/F_{\rm J} > 10^{-4}$, while older stars tend to fall below this threshold. EPIC 247267267 has a fractional flux density of $F_{\rm NUV}/F_{\rm J} = 1.1 \times 10^{-4}$. Using near-UV photometry from *GALEX* and near-IR photometry from 2MASS, we estimated the stellar age based on the (NUV-J) and $(J-K)$ colors and the empirical relations presented in Findeisen et al. (2011). Empirical isochrones from that work are shown in Figure 11, along with comparisons to other known young stellar populations. While there is a large amount of scatter in this color–color diagram, particularly for later-type stars, there is a clear qualitative trend of declining NUV flux for older stars. Proposed Upper Sco and Sco-Cen members were selected from the Young Stellar Object Corral (YSOC), Tuc-Hor members were selected from Kraus et al. (2014), and Hyades members were selected from Perryman et al. (1998). The photometry were dereddened using the extinction coefficients of Yuan et al. (2013) and assuming $A(V) = 0.7$ mag for Upper Sco and $A(V) = 0.16$ mag for Sco-Cen.

Spectroscopic indicators: EPIC 247267267 exhibits a weak Hα absorption feature with emission filling in the wings of the line (Figure 10). This is consistent with the model line profiles produced for weakly active dwarf stars in Cram & Mullan (1979). Hα profiles of this type have been observed for some of the most slowly rotating late-type stars in the Pleiades (e.g., the M0 member SK 17; Stauffer et al. 2016), some G-type members of α Per (Stauffer et al. 1989), as well as the M-type

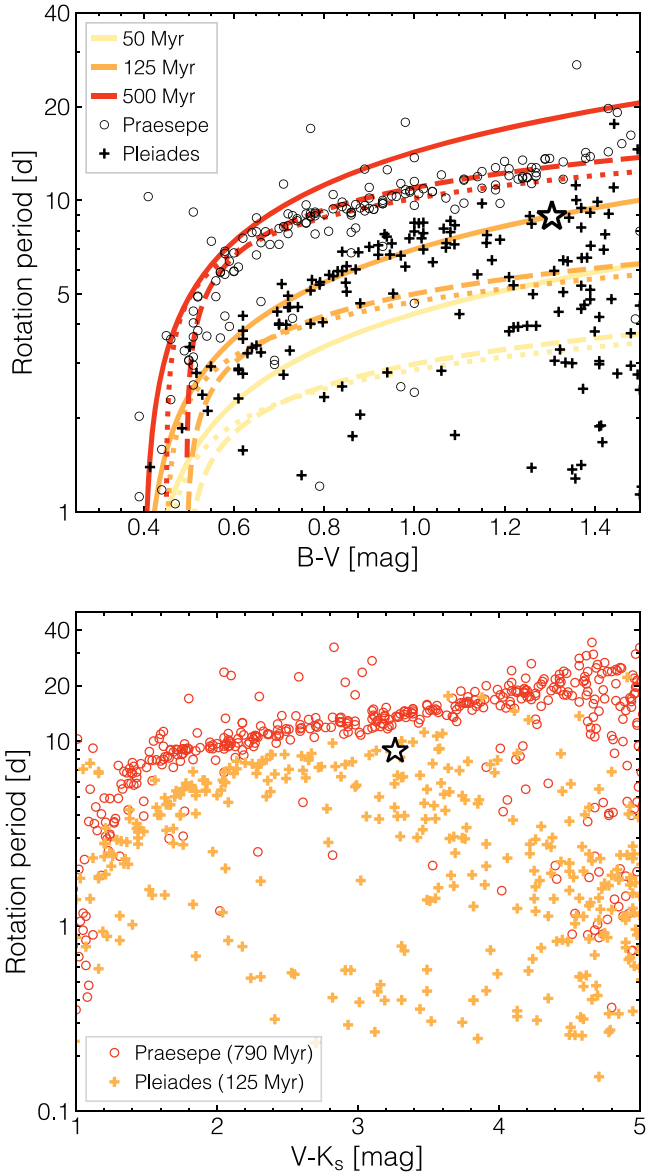

Figure 9. Top: gyrochrones in the period versus $(B - V)$ plane. The solid, dashed, and dotted lines show gyrochrones predicted from Barnes (2007), Mamajek and Hillenbrand (2008), and Angus et al. (2015), respectively. Bottom: Rotation periods versus $(V - K_s)$ color for Praesepe (red) and Pleiades (orange) members. In both figures, the cluster rotation periods are taken from Rebull et al. (2016, 2017), and the white star indicates EPIC 247267267.

Praesepe planet host K2-95 (Obermeier et al. 2016). At the age of the Pleiades, there is a transition at mid-K spectral types where nearly all earlier-type stars show Hα in absorption and at later types nearly all show the line in emission (Stauffer & Hartmann 1987). In α Per, this transition occurs approximately at a spectral type of K6 (Prosser 1992). Thus, the lack of strong Hα emission in EPIC 247267267 is at least consistent with expectations of other stars of a similar mass and age, and in fact some members of Sco-Cen ($\lesssim$20 Myr) with a similar effective temperature also show Hα in absorption (Pecaut & Mamajek 2016). Similar to other late-type stars in young moving groups, EPIC 247267267 exhibits weak emission in other Balmer lines, including Hϵ (seen in Figure 10), Hζ, and Hη.

We do not detect Li I 6708 Å within the spectrum of EPIC 247267267. From the HIRES spectrum, we estimated an upper limit to EW(Li) of $<$20 mÅ. This is not unexpected, given that

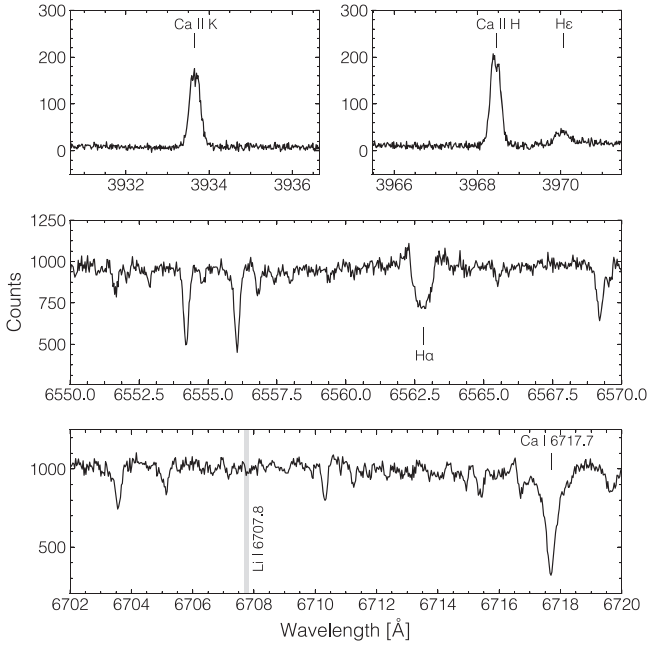

Figure 10. Sections of the HIRES spectra used as age diagnostics. Chromospheric emission in the Ca II H&K lines is clearly detected (top panels), as well as Hϵ emission. The Hα profile shows absorption with emission filling in the wings of the line (middle panel), reminiscent of slowly rotating late-type stars in the Pleiades and some G-type stars in α Per. The Li I 6708 Å absorption line is clearly not present, which is broadly consistent with slowly rotating mid-K dwarfs in the Pleiades and stars of similar $T_{\rm eff}$ in moving groups with ages >20–50 Myr.

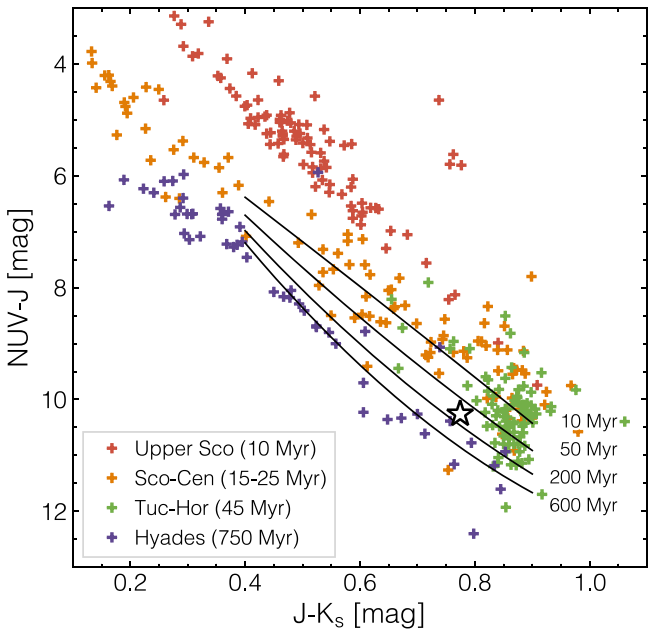

Figure 11. NUV and NIR color–color diagram showing empirical isochrones of Findeisen et al. (2011) and members of young stellar populations. EPIC 247267267 is indicated by the white star.

some late-K dwarfs with ages $\gtrsim$20 Myr are observed to show significant lithium depletion (see Figure 12). Depletion of lithium below detectable levels has been observed in mid- to late-K members of IC 2391 and 2602 ($\sim$50 Myr Barrado y Navascués et al. 2004; Dobbie et al. 2010), AB Dor (149^{+51}_{-19} Myr, Bell et al. 2015), and Tuc-Hor (45 ± 4 Myr, Bell et al. 2015). In the 125 Myr old Pleiades, Soderblom et al. (1993) found that mid- to late-K stars exhibit a wide range of

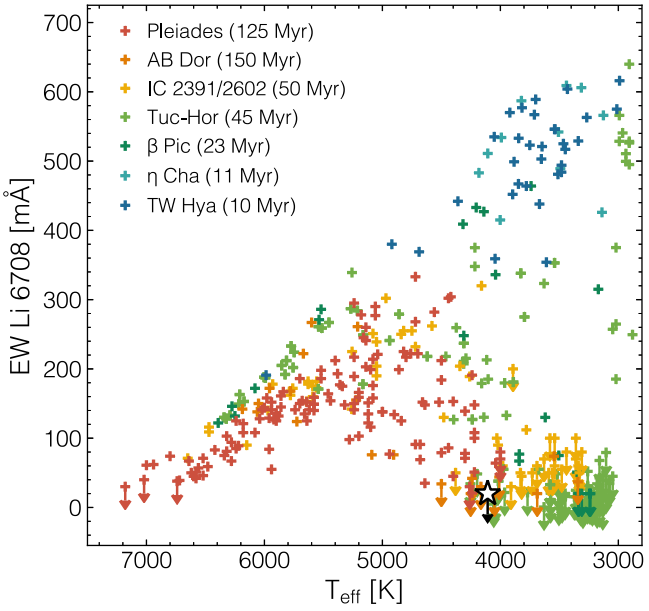

Figure 12. Li I 6708 Å equivalent width versus $T_{\rm eff}$ for members of Pleiades (Soderblom et al. 1993), IC 2391/2602 (Randich et al. 2001), and young moving groups (Mentuch et al. 2008; Kraus et al. 2014). EPIC 247267267 is indicated by the white star.

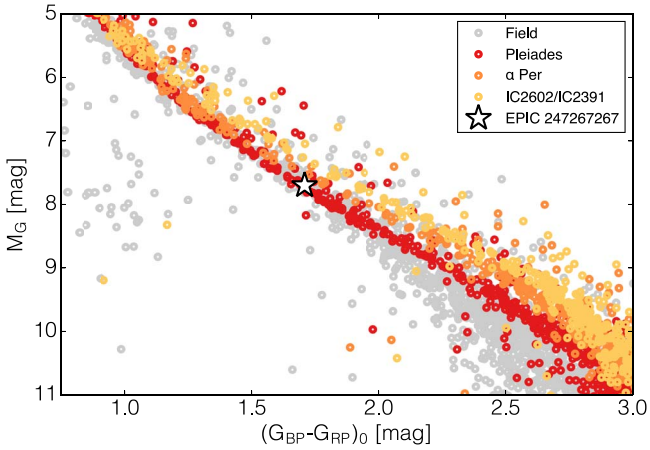

Figure 13. Color–absolute magnitude diagram for EPIC 247267267, as well as young cluster members and field stars, for comparison. EPIC 247267267 is apparently on the main sequence, with an age that is likely older than α Per, IC 2602, or IC 2391, but consistent with the locations of Pleiades members and field stars.

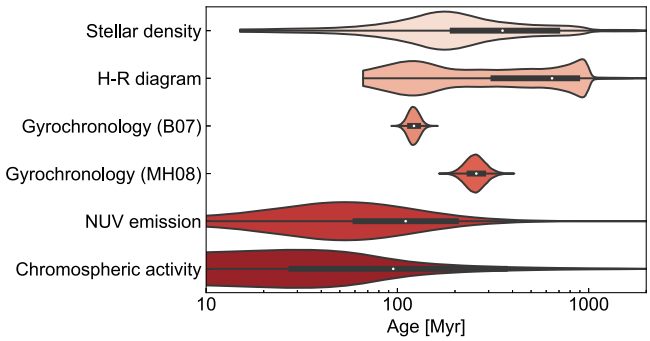

Figure 14. Violin plot demonstrating the kernel density estimates for stellar age distributions resulting from the different age-dating methods discussed in Section 3.5.

Li I 6708 Å equivalent widths, of approximately 20–300 mÅ. Furthermore, at the age of the Pleiades, some stars of a similar mass or color to EPIC 247267267 have yet to spin down. Bouvier et al. (2017) have found that more slowly rotating Pleiads in a given mass range also tend to have weaker lithium absorption. Considered together, the rotation and lithium properties of EPIC 247267267 are consistent with Pleiades-aged or younger mid- to late-K dwarfs. In Figure 12 we show the distribution of Li I 6708 Å equivalent width measurements as a function of $T_{\rm eff}$ for members of young moving groups and clusters.

H-R diagram and stellar density: Since the star is on or very nearly on the main sequence, where evolution is slow for these low-mass stars, isochronal age estimates carry large uncertainties. Nevertheless, as we estimated the mass from interpolation between the PARSECv1.2S models (Bressan et al. 2012; Chen et al. 2014), we also estimated the age in the theoretical H-R diagram using the spectroscopic $T_{\rm eff}$ and the Stefan-Boltzmann luminosity. Because EPIC 247267267 is expected to be near or on the main sequence, the mean stellar density from the transit fits is also not particularly useful for constraining the stellar age, in part due to the fact that the impact parameter is not tightly constrained by the *K2* data. Regardless, we also estimated the stellar age from the directly determined stellar density distribution (from the eccentric orbit transit fit discussed in Section 3.1), a normal distribution in $T_{\rm eff}$, and the PARSECv1.2S models. Though not very precise, the isochronal age estimates (through the H-R diagram or the mean stellar density) do provide a consistent lower limit of 30–70 Myr. From the lack of lithium, it is very unlikely the star is as young as the β Pic moving group (23 ± 3 Myr, Mamajek & Bell 2014). With respect to the lithium levels in other young low-mass stars, ages corresponding to the moving groups Tuc-Hor (Kraus et al. 2014), AB Dor (Mentuch et al. 2008), or the clusters IC 2391/2602 (Randich et al. 2001) would seem plausible. However, the color–absolute magnitude diagram analysis presented as follows suggests such young ages are unlikely. Isochronal age estimates are notoriously uncertain for main-sequence stars, and the age distributions resulting from both our H-R diagram and stellar density analyses are highly skewed with long tails to old ages but very clear peaks around ~100 Myr. To account for this, the isochronal ages we quote in Table 4 are the *modes* of the distributions resulting from the Monte Carlo error analysis, with the lower and upper bounds given by the 1% and 67% percentiles. We found this choice more adequately describes the bulk of the probability density around the peaks of each distribution. For comparison, the median, 16th, and 84th percentiles of the age distributions are 650^{+280}_{-460} Myr and 430^{+1000}_{-260} Myr, for the H-R diagram and stellar density analyses, respectively.

Color–absolute magnitude diagram: We placed EPIC 247267267 in a color–absolute magnitude diagram using the *Gaia* photometry and parallax, and compared it with the positions of young cluster members from Gaia Collaboration et al. (2018a). For comparison, we also included "field" stars observed by the *K2* mission (Figure 13). The field star data were collected from the *Gaia-K2* cross-match compiled by Megan Bedell.[22] From this empirical analysis, we conclude that EPIC 247267267 is likely older than α Per (~70 Myr).

[22] https://gaia-kepler.fun

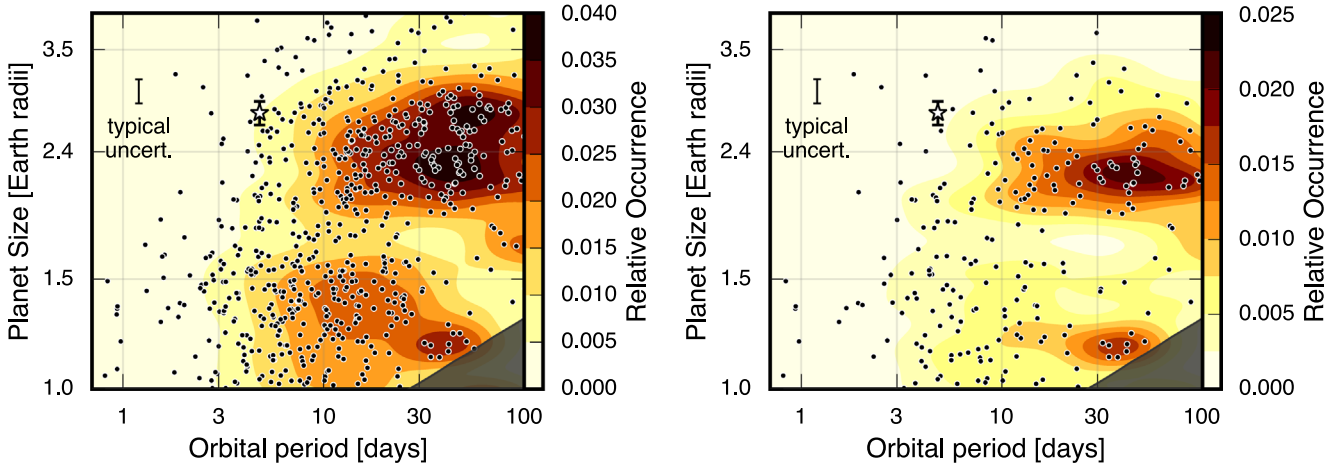

Figure 15. Distribution of small transiting planets in the plane of planet radius and orbital period for the full California-*Kepler* Survey sample, on the left, and only "low-mass" hosts ($<0.97\,M_{\odot}$), on the right. EPIC 247267267 b is indicated by the white star. Overlaid are contours of completeness-corrected occurrence rates (Fulton et al. 2017; Fulton & Petigura 2018).

In Table 4, we report several determinations of the host star age derived through the different methods described previously. We also show the resulting age distributions from these methods and Monte Carlo error propagation in the various input parameters in Figure 14. While the age indicators discussed previously are statistical in nature, they present a consistent picture of a star that is (1) on or very nearly on the ZAMS, (2) unlikely to be as young as the youngest moving groups in the solar neighborhood, and (3) almost certainly younger than the Hyades or Praesepe. The H-R diagram and stellar density analyses are not precise age indicators in this case, but they at least present consistent lower limits to the age of >30–40 Myr (at 68% confidence) or >10 Myr (at 95% confidence). Due to the large uncertainty in $\log R'_{HK}$, our chromospheric activity age distributions also have long tails to unrealistically old ages, but we can still derive lower limits of >20 Myr (at 68% confidence) or >10 Myr (at 95% confidence). The NUV emission levels suggest an age of 45–270 Myr at 68% confidence or 20–640 Myr at 95% confidence, though we note the Findeisen et al. (2011) study calibrated the NUV/NIR age relations using cluster ages that have since been revised. Our tightest age constraints result from the gyrochronology relations, which suggest 95% confidence intervals in age of 100–160 Myr or 200–350 Myr, depending on the preferred calibration.

Considered collectively, these independent age estimates are consistent with a stellar age of $\tau_* = 120^{+640}_{-20}$ Myr (corresponding to the mode and 68% confidence interval of the age distribution resulting from combining each of the different methods and weighting them equally). The long tail toward older ages is due to the H-R diagram and stellar density analyses, as well as the uncertain $\log R'_{HK}$ value. Prior to the release of *Gaia* DR2, the kinematics of EPIC 247267267 were suggestive of membership to the Cas-Tau association. However, the newly available parallax suggests this interpretation is unlikely, and we leave a detailed investigation on the existence, membership, and substructure of the Cas-Tau association to a future work. Nevertheless, EPIC 247267267 is clearly young, with an age that is likely close to that of the Pleiades.

4. Discussion

At first glance, EPIC 247267267 b appears fairly typical when compared with other transiting sub-Neptunes receiving similar incident flux. That is, EPIC 247267267 b does not reside in a region of particularly low occurrence in the plane of planet radius and insolation flux (see Figure 10 of Fulton et al. 2017). Thus, at least some young (<1 Gyr) sub-Neptunes superficially resemble the statistically older population uncovered by *Kepler*. This much was known for slightly more mature planets in the ≃600–800 Myr old Hyades and Praesepe clusters, and we can now extend this conclusion to younger ages.

However, the stars in the California-*Kepler* Survey are all more massive than EPIC 247267267 (Petigura et al. 2017). When compared to other small transiting planets around low-mass stars, EPIC 247267267 b does appear to reside in the large-radius tail of the size distribution for close-in sub-Neptunes. This is apparent in both the planet radius versus period and planet radius versus insolation flux planes for low-mass hosts (Figures 15 and 16). In this case, it seems clear the *K2* photometry of EPIC 247267267 is sensitive to planets much smaller than EPIC 247267267 b, though injection and recovery tests would be needed to quantify how sensitive the data are. In any event, while we cannot be sure that the relatively large size of EPIC 247267267 b is due to its young age, it at least does not appear to be merely a consequence of observational bias.

Other transiting planets around young, low-mass stars also appear to be uncharacteristically large (Figure 16), which has now been pointed out numerous times (e.g., David et al. 2016b; Mann et al. 2016; Obermeier et al. 2016) due to the discovery of more than a dozen transiting planets around stars in clusters and associations from *K2* photometry. However, most transiting planets found around young cluster or field stars of earlier spectral types do not appear to be clear outliers in the period–radius diagram (e.g., Ciardi et al. 2017; Mann et al. 2017b; David et al. 2018; Livingston et al. 2018a), with the notable exception of the apparently single planet K2-100 b (Mann et al. 2017a).

Why might young planets around low-mass stars appear as outliers in the period–radius diagram, while planets of the same age around earlier-type stars seem to reflect the field planet population? One possible explanation for this observed

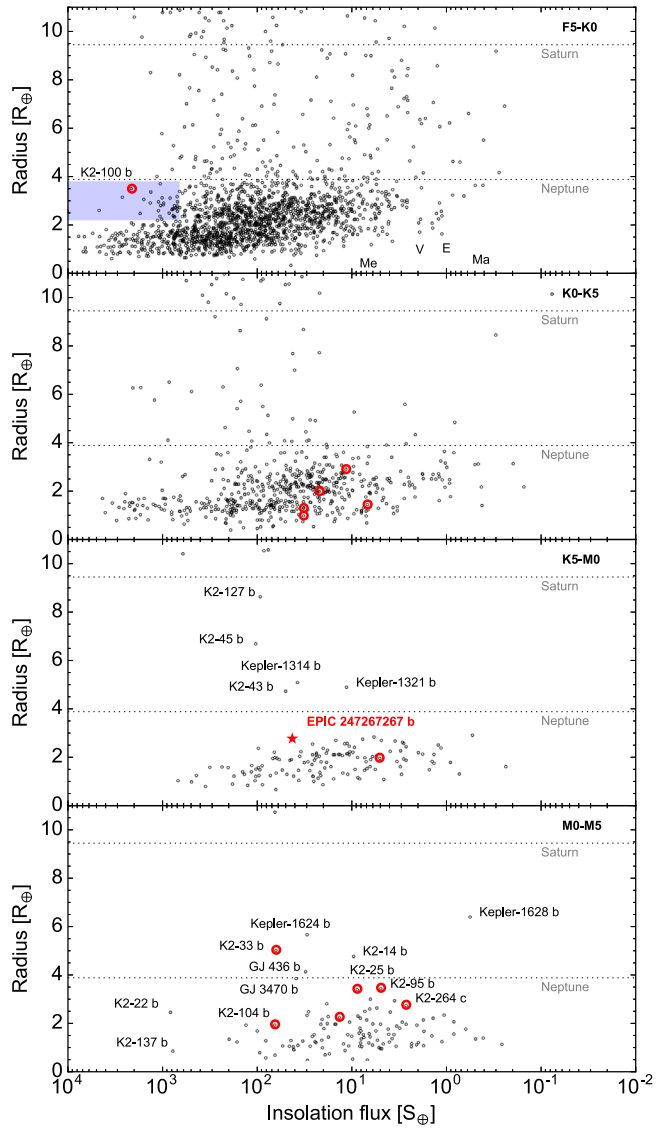

Figure 16. Distribution of confirmed, small transiting planets from the NASA Exoplanet Archive (Akeson et al. 2013) in the plane of planet radius and insolation flux. Planets transiting stars in clusters or associations are circled in red. EPIC 247267267 b is indicated by the red star. Each panel corresponds to a different range in host star spectral type (annotated at top right). EPIC 247267267 b is on the larger end of known, close-in sub-Neptunes around stars of a similar spectral type. A number of other planets orbiting cool young cluster stars also appear to be anomalously large. The blue region in the top panel indicates the hot planet desert described in Lundkvist et al. (2016).

behavior is provided by the theory of photoevaporation. In the photoevaporation framework, atmospheric escape is driven by X-ray and EUV radiation from the host star. A relevant quantity for interpreting the photoevaporation history of any given planet is thus the time-integrated X-ray exposure, more so than the current bolometric insolation, as pointed out in Owen & Wu (2013). A star's X-ray luminosity is highest when it is young and the X-ray emission is in the so-called saturated regime ($L_X/L_{bol} \sim 10^{-3}$, Güdel 2004). After about 100 Myr, corresponding to a typical pre-main-sequence lifetime, a star's X-ray luminosity declines steeply with age (Jackson et al. 2012; Tu et al. 2015). Relative to solar-type stars, low-mass stars are observed to saturate at higher values of L_X/L_{bol} (Jackson et al. 2012), and thus they are expected to be more efficient at eroding planetary atmospheres, with an efficiency that scales as M_*^{-3} at a fixed F_{bol} (Lopez & Rice 2016, and references therein). As a result, the maximum planet radius at a given bolometric exposure varies substantially across different spectral types, while the maximum radius at a given X-ray exposure appears to be less sensitive to the host-star type, as shown by Owen & Wu (2013) and discussed further in Hirano et al. (2018).

However, it is also important to keep in mind that important degeneracies likely influence observed exoplanet populations. For example, it has been shown for solar-type stars that the occurrence of warm sub-Neptunes is higher for metal-rich stars (Petigura et al. 2018). Notably, the Hyades and Praesepe clusters, where some of the anomalously large, young transiting planets have been found, are significantly metal-rich (Pace et al. 2008; Cummings et al. 2017). Thus, in order to separate age-dependent and metallicity-dependent trends in, for example, planetary radii, one must compare the planet populations in these clusters to field stars of a similar metallicity. Additionally, Fulton & Petigura (2018) have recently examined the stellar-mass dependence of the radius gap using high-precision stellar radii enabled by *Gaia* parallaxes. Those authors find evidence that the bimodal distribution of planet sizes shifts to smaller sizes around later-type stars, which might indicate that low-mass stars produce smaller planet cores. Thus, differences in the sizes of planets around low-mass and solar-type stars may reflect scalings not only in the photoevaporation efficiency, but also in the initial core-mass function. The best way to bring clarity to these issues is through the characterization of larger samples of exoplanets around stars that exhibit a wide range of diversity in mass, metallicity, and age.

It is also notable that the young planets that appear most clearly as outliers in the period–radius plane are all apparently single-planet systems (K2-25 b, K2-33 b, K2-95 b, K2-100 b, EPIC 247267267 b), while those that appear more similar to the field planet population occur in multi-planet systems (K2-136, K2-233, K2-264). However, the statistics are simply too small to make a meaningful conclusion about the differences between young single- and multi-planet systems at this point.

Ultimately, a comparison between the typical densities of young and old planets may be more elucidating than simply comparing radii. This requires a determination of the planet's mass. From the planet radius distribution, we calculated a predicted mass for EPIC 247267267 b of $8.5^{+6.4}_{-3.8}\,M_\oplus$ using the `forecaster`[23] tool in PYTHON, which is based on the Chen & Kipping (2017a) mass–radius relations for exoplanets. For this range of plausible planet masses and the stellar mass we adopt, we calculated an expected Doppler semi-amplitude of 2.4–7.7 m s^{-1}. Notably, existing exoplanet mass–radius relations are calibrated using field-aged planets. If sub-Neptunes as young as EPIC 247267267 b are less dense at early times, then the true Doppler amplitude may be on the lower end of the range quoted. While the expected Doppler amplitude is within reach of current precision RV instruments, the relatively high stellar activity will likely present challenges. Given the measured chromospheric activity level for EPIC 247267267, it is likely the RV jitter is greater than 30 m s^{-1} and possibly larger than 100 m s^{-1} (Hillenbrand et al. 2015). The RV jitter may also be approximated from the amplitude of photometric variability and $v \sin i_*$, from the equation $\sigma_{RV} = \mathrm{rms}_{K2} \times v \sin i_*$, which yields 33 m s^{-1}, considerably larger than the expected signal

[23] https://github.com/davidkipping/forecaster

from the planet. Since the star is brighter and activity should be lower at infrared wavelengths, it would be advantageous to measure the planet's mass with an IR precision spectrograph such as the PARVI instrument planned for Palomar Observatory, or one of many other spectrographs in operation or development (Plavchan et al. 2015).

Interestingly, no transiting planets have yet been confirmed in the Pleiades, despite systematic searches within the *K2* data of ~1000 members (Gaidos et al. 2017; Rizzuto et al. 2017). A single candidate was reported by Rizzuto et al. (2017), but the planet has not yet been validated, and the probability of Pleiades membership was estimated to be 62%. By comparison, eight confirmed transiting planets and one candidate have been reported in Praesepe (Libralato et al. 2016; Obermeier et al. 2016; Mann et al. 2017a; Pepper et al. 2017; Livingston et al. 2018b; Rizzuto et al. 2018), a cluster with a distance and metallicity not much different from the Pleiades and for which a similar number of members were observed by *K2*. In the Hyades, four transiting planets around two hosts have been found in a search of <200 members (David et al. 2016a; Mann et al. 2016, 2017b; Ciardi et al. 2017; Livingston et al. 2018a), in addition to a single-transit planet candidate (Vanderburg et al. 2018). An important difference between the clusters is that at the age of the Pleiades, most members are spinning as rapidly as they ever will, while Praesepe and Hyades stars have spun down considerably and are thus more amenable to transit searches. It is also possible that the Pleiades members show enhanced photometric activity (in the form of larger and more frequent flares, larger variability amplitudes, and/or more rapidly evolving spot patterns), making the removal of these trends more difficult. It may be tempting to ascribe the lack of planets in the Pleiades (to this point) to some physical mechanism, such as ongoing orbital migration or differences in the cluster environments. However, with an age unlikely to be much older than the Pleiades, the case of EPIC 247267267 b highlights the importance of taking a holistic approach toward the comparison of planet occurrence rates at young and old ages.

5. Conclusions

We report the discovery of EPIC 247267267 b, a transiting sub-Neptune orbiting a young ($\tau = 120^{+640}_{-20}$ Myr), low-mass star. The kinematics of EPIC 247267267 prior to *Gaia* DR2 were suggestive of membership to the poorly studied Cas-Tau association, which we examined here. However, the *Gaia* parallax places the star at a distance that seems to be incompatible with that interpretation. Nevertheless, through a detailed stellar age analysis using multiple indicators of youth, we were able to find evidence for a self-consistent Pleiades-like age that suggests the planet host may be a zero-age main-sequence star.

The collection of young transiting planets provides important benchmarks for photoevaporation models, which predict the mass-loss evolution of close-in planets. The majority of photoevaporation-driven mass loss is expected to occur within the first ~100 Myr of a star's life, when stellar XUV fluxes are highest and when the planet's surface gravity is expected to be lower due to ongoing contraction (Lopez & Fortney 2013; Owen & Wu 2013). Observing photoevaporation in action requires a sample of young transiting planets around relatively bright stars and an effective probe of atmospheric escape. As discussed in Section 4, it will be necessary to use one of the new generation NIR spectrographs to measure the mass of EPIC 247267267 b.

Finally, young exoplanets are useful for constraining migration scenarios and timescales. Presently, it is unclear *when* the population of close-in planets assembled. By refining the ages of known exoplanet host stars and surveying young stellar populations with greater intensity, it may be possible to observe temporal evolution in the orbital properties (periods, eccentricities, obliquities) of exoplanets. Any such evolutionary trends could provide important clues about the dynamical histories and formation scenarios of close-in exoplanets.

This research was carried out at the Jet Propulsion Laboratory, California Institute of Technology, under a contract with the National Aeronautics and Space Administration. We thank the anonymous referee for comments which improved this manuscript. T.J.D. and E.E.M. acknowledge support from the Jet Propulsion Laboratory Exoplanetary Science Initiative. M.B. acknowledges support from the North Carolina Space Grant Consortium. This work was performed in part under contract with the California Institute of Technology (Caltech)/Jet Propulsion Laboratory (JPL) funded by NASA through the Sagan Fellowship Program executed by the NASA Exoplanet Science Institute. This paper includes data collected by the *Kepler* mission. Funding for the *Kepler* mission is provided by the NASA Science Mission directorate. Some of the data presented in this paper were obtained from the Mikulski Archive for Space Telescopes (MAST). STScI is operated by the Association of Universities for Research in Astronomy, Inc., under NASA contract NAS5-26555. Support for MAST for non-*HST* data is provided by the NASA Office of Space Science via grant NNX09AF08G and by other grants and contracts. Some of the data presented herein were obtained at the W. M. Keck Observatory, which is operated as a scientific partnership of the California Institute of Technology, the University of California, and the National Aeronautics and Space Administration. The observatory was made possible by the generous financial support of the W. M. Keck Foundation. The authors wish to recognize and acknowledge the very significant cultural role and reverence that the summit of Maunakea has always had within the indigenous Hawaiian community. We are most fortunate to have the opportunity to conduct observations from this mountain. This research has made use of the VizieR catalog access tool, CDS, Strasbourg, France. The original description of the VizieR service was published in A&AS 143, 23. The Pan-STARRS1 Surveys (PS1) and the PS1 public science archive have been made possible through contributions by the Institute for Astronomy, the University of Hawaii, the Pan-STARRS Project Office, the Max Planck Society and its participating institutes, the Max Planck Institute for Astronomy, Heidelberg and the Max Planck Institute for Extraterrestrial Physics, Garching, The Johns Hopkins University, Durham University, the University of Edinburgh, the Queen's University Belfast, the Harvard-Smithsonian Center for Astrophysics, the Las Cumbres Observatory Global Telescope Network Incorporated, the National Central University of Taiwan, the Space Telescope Science Institute, the National Aeronautics and Space Administration under grant No. NNX08AR22G issued through the Planetary Science Division of the NASA Science Mission Directorate, the National Science Foundation grant No. AST-1238877, the University of Maryland, Eotvos Lorand

University (ELTE), the Los Alamos National Laboratory, and the Gordon and Betty Moore Foundation. This work has made use of data from the European Space Agency (ESA) mission *Gaia* (https://www.cosmos.esa.int/gaia), processed by the *Gaia* Data Processing and Analysis Consortium (DPAC, https://www.cosmos.esa.int/web/gaia/dpac/consortium). Funding for the DPAC has been provided by national institutions, in particular the institutions participating in the *Gaia* Multilateral Agreement.

Facilities: FLWO:1.5 m (TRES), Keck:I (HIRES), Keck:II (NIRC2), *Kepler*, PS1, Shane (ShARCS).

Software: emcee (Foreman-Mackey et al. 2013), forecaster (Chen & Kipping 2017b), isoclassify (Huber et al. 2017), k2sc (Aigrain et al. 2016), k2sff (Vanderburg & Johnson 2014), pytransit (Parviainen 2015), radvel (Fulton et al. 2018), vespa (Morton 2015).

Appendix
The Cas-Tau Association and Its Turnoff Age

Cas-Tau was first formally proposed as an association by Blaauw (1956), based on the common motions of 49 B-stars covering a remarkably large patch of sky of about $100^\circ \times 140^\circ$. The association shares motions with and spatially surrounds the α Persei (Per OB3) cluster, which led Blaauw to suggest a common origin for the two groups. Indeed, Rasmuson (1921) had already noted the kinematic group was not limited to the central α Per cluster, but that several other B- and A-stars formed a co-moving stream extending well beyond the cluster core. In the years following Blaauw's work, the status of Cas-Tau as a *bona fide* moving group was debated in the literature on the basis of radial velocities (Petrie 1958) and large scatter in the color-Hβ relation (Crawford 1963). However, based on *Hipparcos* parallaxes, de Zeeuw et al. (1999) concluded that Cas-Tau is indeed a physical association that likely shares a common origin with α Per, though only a third of Blaauw's original sample were finally regarded as members.

Today, the low-mass membership of Cas-Tau remains essentially unknown. An X-ray survey in the direction of Taurus found evidence for a population of stars that are older and more widely distributed than the CTTS in the Taurus-Auriga star formation complex (Walter et al. 1988). Those authors found that this distributed older population outnumbers the CTTS population by a factor of 10:1, and there are suggestions that this older population includes members of the Cas-Tau association (Hartmann et al. 1991; Walter & Boyd 1991). Assuming that all of Blaauw's original B-stars are indeed Cas-Tau members, Hartmann et al. (1991) argued based on expectations from the initial mass function that the projected surface density of members with masses $\gtrsim 0.8\,M_\odot$ should be about 0.2 per square degree. In hindsight, this may be an overestimate, given that the *Hipparcos* study found many of Blaauw's original sample are not likely to be members. Nevertheless, within the *K2* Campaign 13 field, one might expect a couple dozen members in this mass range and an even larger number of lower-mass members. Since the area of Cas-Tau is so large in the sky, additional members might have plausibly been observed during other *K2* campaigns.

The precise age of Cas-Tau is not well known, in part due to our incomplete knowledge of the low-mass members. From the kinematics of the originally proposed members, Blaauw (1956) derived an expansion age for Cas-Tau in the range of 50–70 Myr. Due to the common kinematics between the associations, it is generally believed that Cas-Tau is younger than or coeval with α Per. Early examinations of the main-sequence turnoff for α Per found ages of 50 Myr using models with no convective overshoot (Mermilliod 1981; Meynet et al. 1993). The age of α Per has since been refined using the lithium depletion boundary (LDB) technique, with estimates of 90 ± 10 Myr (Stauffer et al. 1999), 85 ± 10 Myr (Barrado y Navascués et al. 2004), and most recently $80 \pm 11 \pm 4$ Myr (Soderblom et al. 2014). The LDB ages are broadly consistent with age estimates of 80 Myr from a CMD of the lower main sequence (Prosser 1992); 80 Myr from a CMD of the upper main sequence, using models with moderate convective overshoot (Ventura et al. 1998); and 70 Myr from an H-R diagram of the upper main sequence (David & Hillenbrand 2015).

To our knowledge, the only determination of a turnoff age for Cas-Tau is the estimate of 20–30 Myr from de Zeeuw and Brand (1985). Motivated by our suggestion that the planet host EPIC 247267267 belongs to the association, we derive a new turnoff age here. We began with the list of 83 B- and A-type members, listed in Table 5, proposed by de Zeeuw et al. (1999). For each of the proposed members, we gathered trigonometric parallaxes from the *Gaia* TGAS catalog (Gaia Collaboration et al. 2016a, 2016b) when available and from the Extended *Hipparcos* compilation otherwise (XHIP; Anderson & Francis 2012). For each star, we then gathered *UBV* photometry from Mermilliod (2006) and *uvbyβ* photometry from Paunzen (2015). Of the 83 proposed members, 19 stars were missing both *UBV* and *uvbyβ* photometry from the aforementioned compilations, while 5 stars lacked only the *UBV* data and 11 stars lacked only the *uvbyβ* data. Nearly all of the stars missing photometry have spectral types of B8 or later, and given that we determine the main-sequence turnoff to be around spectral type B2 for Cas-Tau, these stars contribute little information to the turnoff age anyhow. Our motivation for including both *UBV* and *uvbyβ* photometry was for the purpose of consistency checks. We ultimately derived the turnoff age from *UBV* photometry, so stars missing those data were excluded from our analysis, and any star that lacked both *UBV* and *uvbyβ* photometry was not included in our various consistency checks described as follows. To guide our analysis, we additionally gathered spectral types from Skiff (2014), and $v \sin i$ measurements and multiplicity information from Abt et al. (2002). For each star, we also performed literature searches for further information on multiplicity and to vet for EBs.

Many of the proposed members are reddened. We determined the amount of reddening for each star using the *UBV* photometry and the revised Q-method presented in Pecaut & Mamajek (2013). For those stars with *uvbyβ* photometry, we used the iterative dereddening scheme of Shobbrook (1983) to determine an independent value for the extinction. Among the stars with both sets of photometry, we found the $A(V)$ values derived from the Q-method and the *uvbyβ* iterative method to be well-described by a one-to-one relation with a scatter of 0.066 mag. From an empirical relation between $(b-y)_0$ and $(B-V)_0$ for B-type stars (Crawford 1978), we also compared the intrinsic $(B-V)$ colors from the two different dereddening methods and found these to be in good agreement with a scatter of 0.01 mag. We ultimately used the intrinsic colors and $A(V)$ values from the *UBV* photometry, but we adopted 0.01 mag as the uncertainty in $(B-V)_0$ for our turnoff age analysis to account for the different estimates provided by the *uvbyβ* photometry.

Table 5
Proposed Cas-Tau Members

Name	HIP	Prob. (%)	SpT	ϖ (mas)	V (mag)	M_V (mag)	$B-V$ (mag)	$U-B$ (mag)	$(B-V)_0$ (mag)	$(U-\mathrm{B})_0$ (mag)	$E(B-V)$ (mag)	A_V (mag)
HD 1976	1921	100	B5IV	3.26 ± 0.63	5.571 ± 0.015	−1.912 ± 0.473	−0.122 ± 0.009	−0.603 ± 0.010	−0.171 ± 0.004	−0.637 ± 0.015	0.049 ± 0.012	0.159 ± 0.038
HD 2626	2377	100	B9IIIn	4.24 ± 0.5	5.942 ± 0.004	−0.913 ± 0.261	0.006 ± 0.007	−0.359 ± 0.003	−0.126 ± 0.002	−0.453 ± 0.007	0.132 ± 0.008	0.431 ± 0.027
13 Cas	2474	98	B6V	4.29 ± 0.28	6.170	−0.676 ± 0.146	−0.100	−0.480	−0.138 ± 0.003	−0.506 ± 0.015	0.039 ± 0.012	0.127 ± 0.039
λ Cas	2505	80	B8Vnn	8.64 ± 0.43	4.749 ± 0.054	−0.572 ± 0.118	−0.101 ± 0.004	−0.340 ± 0.020	−0.101 ± 0.004	−0.340 ± 0.020	0.000	0.000
HD 2974	2647	97	B8:	4.04 ± 0.4	7.897 ± 0.009	0.923 ± 0.217	−0.007 ± 0.005	−0.210	−0.084 ± 0.003	−0.266 ± 0.013	0.077 ± 0.007	0.251 ± 0.021
HD 3291	2866	97	B9	3.64 ± 0.45	…	…	…	…	…	…	…	…
omi Cas	3504	99	B5III	4.64 ± 0.38	4.573 ± 0.046	−2.107 ± 0.187	−0.069 ± 0.009	−0.512 ± 0.016	−0.154 ± 0.005	−0.571 ± 0.021	0.084 ± 0.012	0.275 ± 0.039
HD 5409	4437	99	B9V	3.2 ± 0.54	7.852 ± 0.015	0.326 ± 0.398	0.038 ± 0.022	…	…	…	…	…
HR 302	5062	100	B3V	2.48 ± 0.45	6.528 ± 0.013	−1.544 ± 0.419	−0.081 ± 0.010	−0.579 ± 0.061	−0.173 ± 0.020	−0.642 ± 0.074	0.092 ± 0.023	0.299 ± 0.075
HR 342	5566	51	B9.5V	8.06 ± 0.32	5.551 ± 0.011	0.083 ± 0.087	−0.066 ± 0.004	−0.135 ± 0.158	−0.066 ± 0.004	−0.135 ± 0.158	0.000	0.000
HD 7349	5813	97		3.5 ± 0.64	…	…	…	…	…	…	…	…
HD 8346	6480	99	A0V	7.2 ± 0.39	…	…	…	…	…	…	…	…
HD 9709	7457	98	B7IV/Vne[a]	3.13 ± 0.58	7.070	−0.513 ± 0.416	−0.050	−0.430	−0.134 ± 0.003	−0.490 ± 0.015	0.084 ± 0.012	0.276 ± 0.040
HD 10404	7988	88	B8IV	3.54 ± 0.52	…	…	…	…	…	…	…	…
ϕ Per	8068	100	B1.5V:e[a]	4.54 ± 0.2	4.062 ± 0.012	−2.655 ± 0.092	−0.042 ± 0.007	−0.935 ± 0.012	−0.318 ± 0.004	−1.131 ± 0.015	0.276 ± 0.009	0.891 ± 0.030
HD 10577	8108	100	B9V	3.76 ± 0.58	7.020	−0.133 ± 0.349	0.020	−0.210	−0.089 ± 0.003	−0.290 ± 0.015	0.109 ± 0.012	0.357 ± 0.040
4 Ari	8387	54	B9.5V	11.85 ± 0.25	5.860	1.228 ± 0.046	−0.037 ± 0.005	−0.133 ± 0.009	−0.053 ± 0.003	−0.144 ± 0.012	0.016 ± 0.007	0.051 ± 0.023
HD 11104	8551	100	B8IV/V	2.23 ± 0.61	…	…	…	…	…	…	…	…
1 Per	8704	98	B2V	2.52 ± 0.33	5.508 ± 0.073	−2.512 ± 0.308	−0.179 ± 0.008	−0.834 ± 0.009	−0.242 ± 0.004	−0.880 ± 0.014	0.063 ± 0.011	0.204 ± 0.034
ϵ Cas	8886	93	B3V	7.92 ± 0.43	3.370 ± 0.009	−2.134 ± 0.117	−0.155 ± 0.007	−0.591 ± 0.014	−0.159 ± 0.005	−0.592 ± 0.018	0.004 ± 0.009	0.014 ± 0.031
HD 12518	9656	100	B9IV	7.09 ± 0.48	6.660	0.910 ± 0.145	−0.030	−0.310	−0.106 ± 0.003	−0.365 ± 0.015	0.076 ± 0.012	0.247 ± 0.040
HD 12844	9890	98		4.7 ± 0.41	…	…	…	…	…	…	…	…
HR 679	10924	99	B5V	4.1 ± 0.37	6.100	−0.836 ± 0.194	−0.080	−0.480	−0.142 ± 0.003	−0.524 ± 0.014	0.062 ± 0.012	0.203 ± 0.040
63 And	10944	89	B9VpSi	8.31 ± 0.34	5.550	0.145 ± 0.092	−0.094 ± 0.029	−0.401 ± 0.017	−0.118 ± 0.007	−0.418 ± 0.031	0.024 ± 0.035	0.079 ± 0.113
BD+67 195	10974	95	B2	4.22 ± 0.26	…	…	…	…	…	…	…	…
HD 14795	11295	99	B5V	4.73 ± 0.32	7.680	1.044 ± 0.145	0.000	−0.410	−0.139 ± 0.003	−0.509 ± 0.015	0.139 ± 0.012	0.453 ± 0.040
HR 760	12218	100	B5V	4.25 ± 0.5	…	…	−0.120 ± 0.000	−0.483 ± 0.005	−0.135 ± 0.002	−0.493 ± 0.010	0.015 ± 0.012	0.048 ± 0.039
HD 16485	12453	99	B9V	3.35 ± 0.39	…	…	…	…	…	…	…	…
HD 16449	12477	100	B9V	3.41 ± 0.39	…	…	…	…	…	…	…	…
BD+65 291	13003	74	B8	5.42 ± 0.25	…	…	…	…	…	…	…	…
HD 17359	13124	93	A0Vs	5.29 ± 0.77	7.563 ± 0.002	1.155 ± 0.321	0.037 ± 0.012	0.065 ± 0.106	0.033 ± 0.077	0.084 ± 0.183	0.004 ± 0.079	0.012 ± 0.263
sig Ari	13327	86	B7V	6.6 ± 0.32	5.480	−0.427 ± 0.107	−0.089 ± 0.002	−0.439 ± 0.012	−0.129 ± 0.003	−0.467 ± 0.014	0.040 ± 0.004	0.129 ± 0.013
HD 17443	13330	100	B9V	3.49 ± 0.25	8.740 ± 0.000	1.448 ± 0.158	0.302 ± 0.010	0.145 ± 0.019	−0.039 ± 0.008	−0.098 ± 0.028	0.341 ± 0.015	1.126 ± 0.050
HR 950	14887	100	B4V	4.99 ± 0.4	…	…	−0.090	−0.570	−0.168 ± 0.004	−0.624 ± 0.015	0.078 ± 0.013	0.253 ± 0.041
HD 19981	15065	75	B9IV	5.86 ± 0.8	…	…	…	…	…	…	…	…
HD 20336	15520	87	B2IV:e	4.28 ± 0.48	4.835 ± 0.028	−2.027 ± 0.247	−0.152 ± 0.014	−0.771 ± 0.013	−0.225 ± 0.006	−0.823 ± 0.020	0.073 ± 0.018	0.235 ± 0.059
HD 20510	15531	98	B9V	5.85 ± 0.38	7.050	0.885 ± 0.142	0.050	−0.140	−0.075 ± 0.004	−0.231 ± 0.015	0.125 ± 0.013	0.411 ± 0.042
τ Ari	15627	100	B5III	6.41 ± 0.73	5.271 ± 0.012	−0.708 ± 0.251	−0.067 ± 0.008	−0.531 ± 0.048	−0.161 ± 0.016	−0.597 ± 0.061	0.094 ± 0.018	0.306 ± 0.060
u Tau	17563	80	B3V	6.11 ± 0.29	5.341 ± 0.020	−0.730 ± 0.103	−0.112 ± 0.004	−0.618 ± 0.008	−0.179 ± 0.003	−0.665 ± 0.011	0.067 ± 0.006	0.216 ± 0.018
HD 23477	17681	98		7.26 ± 0.39	7.066	1.367 ± 0.113	0.010	−0.046	−0.031 ± 0.006	−0.071 ± 0.018	0.041 ± 0.014	0.134 ± 0.046
HR 1147	17707	93	B9Vnn	9.07 ± 0.5	6.100	0.885 ± 0.125	−0.022 ± 0.011	−0.160	−0.066 ± 0.004	−0.193 ± 0.017	0.044 ± 0.014	0.144 ± 0.046
HD 23990	17907	95	B9.5V	7.16 ± 0.51	…	…	…	…	…	…	…	…
V766 Tau	18033	100	B9pSi	6.48 ± 0.55	6.310	0.363 ± 0.194	−0.062 ± 0.012	−0.479 ± 0.013	−0.146 ± 0.005	−0.538 ± 0.019	0.083 ± 0.015	0.272 ± 0.048
HD 23662	18067	97	B8V	5.2 ± 0.48	…	…	−0.080	−0.240	−0.080	−0.240	0.000	0.000
HD 24456	18190	98	B9.5V	7.2 ± 0.37	…	…	…	…	…	…	…	…
HD 26323	19466	82	A2V	6.72 ± 0.34	…	…	…	…	…	…	…	…
HD 26676	19720	73	B8Vn	4.87 ± 0.77	6.225 ± 0.084	−0.362 ± 0.379	0.048 ± 0.004	−0.335 ± 0.014	−0.127 ± 0.004	−0.460 ± 0.017	0.175 ± 0.006	0.574 ± 0.020

Table 5
(Continued)

Name	HIP	Prob. (%)	SpT	ϖ (mas)	V (mag)	M_V (mag)	$B-V$ (mag)	$U-B$ (mag)	$(B-V)_0$ (mag)	$(U-\mathrm{B})_0$ (mag)	$E(B-V)$ (mag)	A_V (mag)
μ Tau	19860	96	B3IV	7.16 ± 0.34	4.280 ± 0.010	−1.453 ± 0.104	−0.060 ± 0.009	−0.522 ± 0.017	−0.160 ± 0.006	−0.594 ± 0.023	0.100 ± 0.013	0.327 ± 0.041
HR 1328	20063	100	B9V	5.06 ± 0.8	6.210	−0.307 ± 0.359	−0.070 ± 0.007	−0.315 ± 0.011	−0.100 ± 0.003	−0.338 ± 0.014	0.030 ± 0.009	0.099 ± 0.028
53 Tau	20171	97	B9Vsp	12.08 ± 0.36	5.350	0.759 ± 0.066	−0.092 ± 0.019	−0.274 ± 0.015	−0.092 ± 0.019	−0.274 ± 0.015	0.000	0.000
HD 27528	20229	96	A0Vn	5.79 ± 0.41	6.800	0.609 ± 0.157	−0.030	…	…	…	…	…
d Per	20354	100	B4IV	6.43 ± 0.28	4.849 ± 0.010	−1.106 ± 0.097	−0.027 ± 0.010	−0.520 ± 0.012	−0.166 ± 0.004	−0.619 ± 0.017	0.139 ± 0.013	0.454 ± 0.041
HD 27707	20424	96		6.44 ± 0.33	…	…	…	…	…	…	…	…
HR 1415	20884	94	B5V	8.52 ± 0.35	5.545 ± 0.109	0.192 ± 0.138	−0.102 ± 0.004	−0.543 ± 0.005	−0.156 ± 0.002	−0.580 ± 0.007	0.054 ± 0.005	0.176 ± 0.016
HD 28715	21135	100		6.32 ± 0.54	…	…	…	…	…	…	…	…
HD 28796	21177	100		5.04 ± 0.55	…	…	…	…	…	…	…	…
DZ Eri	21192	97	B9IIIpHg	6.86 ± 0.35	5.799 ± 0.020	−0.020 ± 0.109	−0.144 ± 0.011	−0.548 ± 0.016	−0.149 ± 0.005	−0.550 ± 0.022	0.005 ± 0.014	0.017 ± 0.047
HD 29554	21640	86		6.33 ± 0.49	…	…	…	…	…	…	…	…
HD 286987	21973	81	B8	6.01 ± 0.74	…	…	…	…	…	…	…	…
HD 29866	22034	97	B8V	5.28 ± 0.5	6.064 ± 0.023	−0.333 ± 0.207	0.057 ± 0.018	−0.293 ± 0.016	−0.118 ± 0.006	−0.420 ± 0.025	0.177 ± 0.023	0.578 ± 0.074
μ Eri	22109	73	B4IV	6.25 ± 0.19	4.012 ± 0.008	−2.009 ± 0.066	−0.149 ± 0.005	−0.573 ± 0.011	−0.155 ± 0.004	−0.576 ± 0.014	0.006 ± 0.007	0.019 ± 0.022
HD 30122	22128	100	B5III	4.71 ± 0.51	…	…	0.065 ± 0.005	−0.450 ± 0.000	−0.165 ± 0.004	−0.614 ± 0.013	0.230 ± 0.007	0.750 ± 0.022
HD 30409	22415	100	B9V	3.95 ± 0.29	8.310	1.291 ± 0.158	0.070	−0.050	−0.050 ± 0.005	−0.136 ± 0.017	0.120 ± 0.014	0.396 ± 0.046
HD 31799	23130	98		5.51 ± 0.3	…	…	…	…	…	…	…	…
HD 32884	23745	90		5.32 ± 0.76	…	…	…	…	…	…	…	…
η Aur	23767	99	B3V	13.4 ± 0.2	3.172 ± 0.008	−1.193 ± 0.034	−0.178 ± 0.009	−0.669 ± 0.005	−0.180 ± 0.003	−0.669 ± 0.011	0.001 ± 0.012	0.004 ± 0.038
17 Aur	24740	80	B9.5V	7.05 ± 0.61	6.143 ± 0.013	0.368 ± 0.193	−0.059 ± 0.001	−0.136 ± 0.087	−0.059 ± 0.001	−0.136 ± 0.087	0.000	0.000
15 Cam	24836	99	B5V	3.91 ± 0.7	6.120 ± 0.000	−0.967 ± 0.400	−0.024 ± 0.006	−0.479 ± 0.001	−0.154 ± 0.001	−0.571 ± 0.005	0.130 ± 0.007	0.423 ± 0.023
HD 35034	25157	58	B8V	3.38 ± 0.32	8.020	0.647 ± 0.210	0.030	−0.340	−0.125 ± 0.003	−0.451 ± 0.015	0.155 ± 0.012	0.506 ± 0.040
115 Tau	25499	97	B5V	5.94 ± 0.34	5.416 ± 0.008	−0.727 ± 0.123	−0.100 ± 0.001	−0.540 ± 0.000	−0.156 ± 0.003	−0.578 ± 0.012	0.056 ± 0.003	0.181 ± 0.011
116 Tau	25555	62	B9.5Vn	7.69 ± 0.33	…	…	0.010	−0.050	−0.033 ± 0.005	−0.077 ± 0.017	0.043 ± 0.013	0.142 ± 0.044
HD 35785	25561	99		4.64 ± 0.4	…	…	…	…	…	…	…	…
HD 35945	25657	97		5.8 ± 0.69	7.650	1.438 ± 0.268	0.020	−0.120	−0.062 ± 0.004	−0.180 ± 0.016	0.083 ± 0.013	0.273 ± 0.043
118 Tau	25695	84	B8V	7.67 ± 0.73	5.470	−0.121 ± 0.198	−0.045 ± 0.005	−0.174 ± 0.035	−0.064 ± 0.012	−0.187 ± 0.044	0.019 ± 0.013	0.062 ± 0.043
HD 36453	26034	100	B9V	4.07 ± 0.37	6.607 ± 0.033	−0.350 ± 0.207	−0.040 ± 0.028	−0.190	−0.070 ± 0.007	−0.211 ± 0.028	0.028 ± 0.035	0.093 ± 0.113
125 Tau	26640	94	B3IV	7.63 ± 0.33	5.168 ± 0.008	−0.421 ± 0.095	−0.152 ± 0.002	−0.689 ± 0.003	−0.193 ± 0.001	−0.718 ± 0.004	0.041 ± 0.003	0.134 ± 0.009
HD 38670	27421	87	B9Vn	5.97 ± 0.73	6.070	−0.058 ± 0.273	−0.091 ± 0.009	−0.389 ± 0.025	−0.115 ± 0.007	−0.408 ± 0.032	0.025 ± 0.013	0.081 ± 0.042
HD 39114	27723	100	B9.5IV	4.72 ± 1.04	…	…	…	…	…	…	…	…
HD 39285	27746	93		4.8 ± 1.04	…	…	…	…	…	…	…	…
HD 39773	27962	62	A0III	4.18 ± 0.57	6.800	−0.124 ± 0.307	0.000	−0.360	−0.125 ± 0.003	−0.450 ± 0.015	0.125 ± 0.012	0.410 ± 0.040
nu Ori	29038	100	B3IV	6.32 ± 0.33	4.417 ± 0.007	−1.583 ± 0.113	−0.161 ± 0.013	−0.656 ± 0.022	−0.179 ± 0.008	−0.668 ± 0.030	0.019 ± 0.018	0.061 ± 0.057
HD 44172	30180	95	B8	3.05 ± 0.66	7.340 ± 0.000	−0.294 ± 0.507	−0.100 ± 0.000	−0.511 ± 0.010	−0.147 ± 0.004	−0.543 ± 0.015	0.047 ± 0.012	0.152 ± 0.040
HR 2395	31278	98	B5Vn	5.89 ± 0.24	5.092 ± 0.004	−1.060 ± 0.089	−0.145 ± 0.008	−0.559 ± 0.006	−0.152 ± 0.003	−0.562 ± 0.010	0.007 ± 0.010	0.022 ± 0.033

Note.
[a] Shell star.

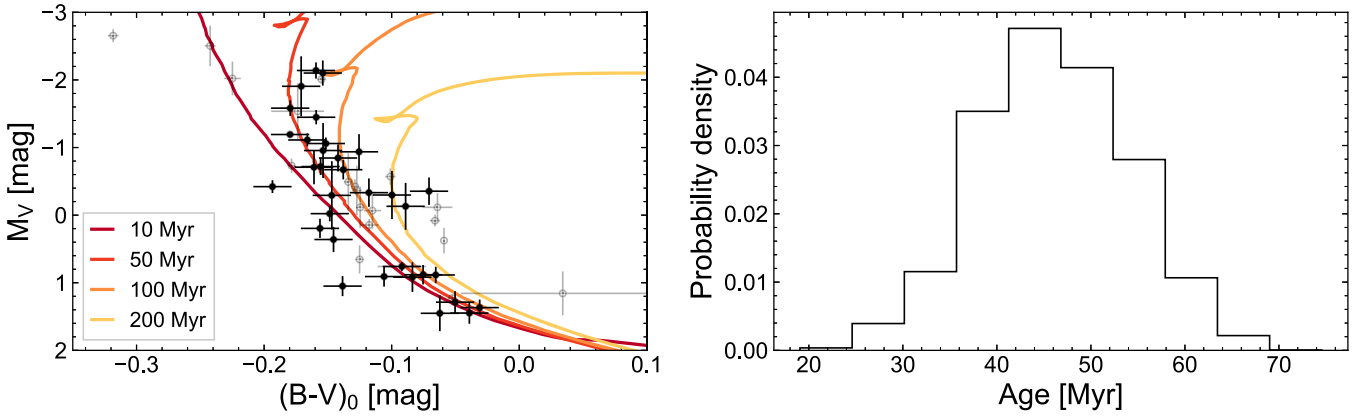

Figure 17. Left: Color–magnitude diagram for proposed members of Cas-Tau. Black points are the high-probability members we used to determine the turnoff age, while the gray points show members that were excluded for the reasons described in the text. Isochrones from the PARSECv1.2S models are indicated by the colored curves. The gray points indicate stars rejected for reasons explained in the text. Right: histogram of turnoff ages resulting from 10^4 Monte Carlo simulations.

Using the intrinsic $(B-V)_0$ colors and M_V magnitudes calculated from the V-band photometry and trigonometric parallaxes, we then proceeded to estimate the turnoff age from comparison with the PARSECv1.2S evolutionary models (Bressan et al. 2012). The uncertainties in the M_V magnitudes were determined from Monte Carlo error estimation, accounting for the uncertainties in V magnitudes and the parallaxes. For high-mass stars such as those considered here, the PARSECv1.2S models are transformed into the observational system through the use of Castelli & Kurucz (2004) model atmospheres, Bessell (1990) *UBVRI* passbands, and the zero points presented in Maíz Apellániz (2006). We used models with a solar metallicity of $Z = 0.0152$ (Caffau et al. 2011) for this analysis.

From the CMD, it is apparent that there is a significant amount of scatter around the turnoff. It is possible that there are interlopers in the de Zeeuw et al. (1999) sample, so in an attempt to address this issue, we considered only stars with membership probabilities $\geqslant$90%, where the probability values originate from those authors. We additionally excluded two high-probability members, because these are emission line stars. These stars are HD 9709 (HIP 7457), a B7IV/Vne shell star, and ϕ Per (HIP 8068), a B1.5V:e shell star and double-lined spectroscopic binary. Furthermore, several of the proposed members are EBs. These stars are 1 Per (HIP 8704), τ Ari (HIP 15627), 17 Aur (HIP 24740), and 15 Cam (HIP 24836).[24] We ultimately excluded 1 Per and 17 Aur on the basis of large eclipse depths (>0.3 mag) and included the other two systems, given their more moderate eclipse depths (Avvakumova et al. 2013). In the course of our analysis, we also found that two of the proposed members are surrounded by reflection nebulae (HD 26676 and HD 17443). Despite the additional extinction, these stars do not appear to be obvious outliers in the CMD and were included in the age analysis.

Using a fine grid of isochrones ($\Delta \log \tau = 0.0025$ dex) with ages between 10^6 and 10^9 yr, we fit an isochrone of each age to the data and evaluated χ^2. We determined the uncertainty on the turnoff age from 10^4 Monte Carlo simulations, in which a new $\chi^2_{\rm min}$ age was calculated from perturbed M_V and $(B-V)_0$ values for each star. In this analysis, the perturbed M_V and $(B-V)_0$ values were drawn from normal distributions in accordance with that star's individual errors. For those stars missing V magnitude error estimates, we assumed an error of 0.01 mag. Ultimately, we found a turnoff age of $\tau_{\rm Cas-Tau} = 46 \pm 8$ Myr, where the value and uncertainty are the median and standard deviation, respectively, of the distribution of ages from the Monte Carlo simulations (Figure 17). This age is in good agreement with the original kinematic estimate of 50–70 Myr from Blaauw (1956), and somewhat younger than the lithium depletion boundary age ($80 \pm 11 \pm 4$ Myr, Soderblom et al. 2014) and turnoff ages derived for the α Per cluster (80 Myr, Ventura et al. 1998).

We note that the analysis provided has not made use of the more precise *Gaia* DR2 parallaxes. A preliminary analysis utilizing the new parallaxes and eliminating the stars HIP 2377, HIP 8387, and HIP 20171 (which appear as outliers in the parallax distribution of proposed members) suggest a slightly older turnoff age of $\tau = 59^{+14}_{-8}$ Myr and reveal a potentially bimodal age distribution. We leave a more detailed study of the age and substructure of this proposed association to a further study.

[24] μ Eri (HIP 22109) is also listed as an EB in SIMBAD, but we did not find published evidence in support of this interpretation in the literature. This star was excluded from the age analysis anyhow, on the basis of its low membership probability.

ORCID iDs

Trevor J. David https://orcid.org/0000-0001-6534-6246
Eric E. Mamajek https://orcid.org/0000-0003-2008-1488
Andrew Vanderburg https://orcid.org/0000-0001-7246-5438
Joshua E. Schlieder https://orcid.org/0000-0001-5347-7062
Erik A. Petigura https://orcid.org/0000-0003-0967-2893
Howard T. Isaacson https://orcid.org/0000-0002-0531-1073
Ann Marie Cody https://orcid.org/0000-0002-3656-6706
John R. Stauffer https://orcid.org/0000-0003-3595-7382
Allyson Bieryla https://orcid.org/0000-0001-6637-5401
David W. Latham https://orcid.org/0000-0001-9911-7388
Benjamin J. Fulton https://orcid.org/0000-0003-3504-5316
Luisa M. Rebull https://orcid.org/0000-0001-6381-515X
Lea A. Hirsch https://orcid.org/0000-0001-8058-7443
Andrew W. Howard https://orcid.org/0000-0001-8638-0320

References

Abt, H. A., Levato, H., & Grosso, M. 2002, ApJ, 573, 359
Aigrain, S., Parviainen, H., & Pope, B. J. S. 2016, MNRAS, 459, 2408
Akeson, R. L., Chen, X., Ciardi, D., et al. 2013, PASP, 125, 989
Anderson, E., & Francis, C. 2012, AstL, 38, 331

Angus, R., Aigrain, S., Foreman-Mackey, D., & McQuillan, A. 2015, MNRAS, 450, 1787
Avvakumova, E. A., Malkov, O. Y., & Kniazev, A. Y. 2013, AN, 334, 860
Barnes, S. A. 2007, ApJ, 669, 1167
Barrado y Navascués, D., Stauffer, J. R., & Jayawardhana, R. 2004, ApJ, 614, 386
Bell, C. P. M., Mamajek, E. E., & Naylor, T. 2015, MNRAS, 454, 593
Bessell, M. S. 1990, PASP, 102, 1181
Blaauw, A. 1956, ApJ, 123, 408
Bouvier, J., Barrado, D., Moraux, E., et al. 2017, arXiv:1712.06525
Bowler, B. P. 2016, PASP, 128, 102001
Boyajian, T. S., von Braun, K., van Belle, G., et al. 2012, ApJ, 757, 112
Brandt, T. D., & Huang, C. X. 2015, ApJ, 807, 24
Bressan, A., Marigo, P., Girardi, L., et al. 2012, MNRAS, 427, 127
Brucalassi, A., Koppenhoefer, J., Saglia, R., et al. 2017, A&A, 603, A85
Brucalassi, A., Pasquini, L., Saglia, R., et al. 2014, A&A, 561, L9
Brucalassi, A., Pasquini, L., Saglia, R., et al. 2016, A&A, 592, L1
Buchhave, L. A., Bizzarro, M., Latham, D. W., et al. 2014, Natur, 509, 593
Buchhave, L. A., Latham, D. W., Johansen, A., et al. 2012, Natur, 486, 375
Caffau, E., Ludwig, H.-G., Steffen, M., Freytag, B., & Bonifacio, P. 2011, SoPh, 268, 255
Cardelli, J. A., Clayton, G. C., & Mathis, J. S. 1989, ApJ, 345, 245
Castelli, F., & Kurucz, R. L. 2004, arXiv:astro-ph/0405087
Chambers, K. C., Magnier, E. A., Metcalfe, N., et al. 2016, arXiv:1612.05560
Chen, H., & Rogers, L. A. 2016, ApJ, 831, 180
Chen, J., & Kipping, D. 2017a, ApJ, 834, 17
Chen, J., & Kipping, D. 2017b, Forecaster: Mass and radii of planets predictor, Astrophysics Source Code Library, ascl:1701.007
Chen, Y., Girardi, L., Bressan, A., et al. 2014, MNRAS, 444, 2525
Choi, J., Dotter, A., Conroy, C., et al. 2016, ApJ, 823, 102
Chubak, C., Marcy, G., Fischer, D. A., et al. 2012, arXiv:1207.6212
Ciardi, D. R., Beichman, C. A., Horch, E. P., & Howell, S. B. 2015, ApJ, 805, 16
Ciardi, D. R., Crossfield, I. J. M., Feinstein, A. D., et al. 2017, arXiv:1709.10398
Claret, A., Hauschildt, P. H., & Witte, S. 2012, A&A, 546, A14
Cochran, W. D., Hatzes, A. P., & Paulson, D. B. 2002, AJ, 124, 565
Cram, L. E., & Mullan, D. J. 1979, ApJ, 234, 579
Crawford, D. L. 1963, ApJ, 137, 523
Crawford, D. L. 1978, AJ, 83, 48
Cumming, A., Butler, R. P., Marcy, G. W., et al. 2008, PASP, 120, 531
Cummings, J. D., Deliyannis, C. P., Maderak, R. M., & Steinhauer, A. 2017, AJ, 153, 128
Cutri, R. M., Skrutskie, M. F., van Dyk, S., et al. 2003, 2MASS All Sky Catalog of Point Sources, https://irsa.ipac.caltech.edu/applications/Gator/
Cutri, R. M., et al. 2013, yCat, 2328, 0
David, T. J., Conroy, K. E., Hillenbrand, L. A., et al. 2016a, AJ, 151, 112
David, T. J., Crossfield, I. J. M., Benneke, B., et al. 2018, AJ, 155, 222
David, T. J., & Hillenbrand, L. A. 2015, ApJ, 804, 146
David, T. J., Hillenbrand, L. A., Petigura, E. A., et al. 2016b, Natur, 534, 658
de Bruijne, J. H. J., & Eilers, A.-C. 2012, A&A, 546, A61
de Zeeuw, P. T., Hoogerwerf, R., de Bruijne, J. H. J., Brown, A. G. A., & Blaauw, A. 1999, AJ, 117, 354
de Zeeuw, T., & Brand, J. 1985, in Birth and Evolution of Massive Stars and Stellar Groups, ed. W. Boland & H. van Woerden (Dordrecht: Reidel), 95
Dobbie, P. D., Lodieu, N., & Sharp, R. G. 2010, MNRAS, 409, 1002
Donati, J. F., Moutou, C., Malo, L., et al. 2016, Natur, 534, 662
Dotter, A. 2016, ApJS, 222, 8
Douglas, S. T., Agüeros, M. A., Covey, K. R., et al. 2016, ApJ, 822, 47
Findeisen, K., & Hillenbrand, L. 2010, AJ, 139, 1338
Findeisen, K., Hillenbrand, L., & Soderblom, D. 2011, AJ, 142, 23
Fischer, D. A., & Valenti, J. 2005, ApJ, 622, 1102
Flewelling, H. A., Magnier, E. A., Chambers, K. C., et al. 2016, arXiv:1612.05243
Foreman-Mackey, D., Hogg, D. W., Lang, D., & Goodman, J. 2013, PASP, 125, 306
Fulton, B. J., & Petigura, E. A. 2018, arXiv:1805.01453
Fulton, B. J., Petigura, E. A., Blunt, S., & Sinukoff, E. 2018, arXiv:1801.01947
Fulton, B. J., Petigura, E. A., Howard, A. W., et al. 2017, AJ, 154, 109
Gagné, J., Mamajek, E. E., Malo, L., et al. 2018, ApJ, 856, 23
Gaia Collaboration, Brown, A. G. A., Vallenari, A., et al. 2016a, A&A, 595, A2
Gaia Collaboration, Babusiaux, C., van Leeuwen, F., et al. 2018a, A&A, 616, A10
Gaia Collaboration, Brown, A. G. A., Vallenari, A., et al. 2018b, arXiv:1804.09365
Gaia Collaboration, Prusti, T., de Bruijne, J. H. J., et al. 2016b, A&A, 595, A1
Gaidos, E., Mann, A. W., Rizzuto, A., et al. 2017, MNRAS, 464, 850
Gilliland, R. L., Brown, T. M., Guhathakurta, P., et al. 2000, ApJL, 545, L47
Girardi, L., Groenewegen, M. A. T., Hatziminaoglou, E., & da Costa, L. 2005, A&A, 436, 895
Gontcharov, G. A. 2006, AstL, 32, 759
Gossage, S., Conroy, C., Dotter, A., et al. 2018, ApJ, 863, 67
Güdel, M. 2004, A&A Rev., 12, 71
Hartmann, L., Stauffer, J. R., Kenyon, S. J., & Jones, B. F. 1991, AJ, 101, 1050
Henden, A. A., Templeton, M., Terrell, D., et al. 2016, yCat, 2336, 0
Hillenbrand, L., Isaacson, H., Marcy, G., et al. 2015, in 18th Cambridge Workshop on Cool Stars, Stellar Systems, and the Sun, ed. G. T. van Belle & H. C. Harris (Cambridge: Cambridge Univ. Press), 759
Hirano, T., Dai, F., Gandolfi, D., et al. 2018, AJ, 155, 127
Howard, A. W., Marcy, G. W., Bryson, S. T., et al. 2012, ApJS, 201, 15
Howell, S. B., Rowe, J. F., Bryson, S. T., et al. 2012, ApJ, 746, 123
Howell, S. B., Sobeck, C., Haas, M., et al. 2014, PASP, 126, 398
Huber, D., Bryson, S. T., Haas, M. R., et al. 2016, ApJS, 224, 2
Huber, D., Zinn, J., Bojsen-Hansen, M., et al. 2017, ApJ, 844, 102
Jackson, A. P., Davis, T. A., & Wheatley, P. J. 2012, MNRAS, 422, 2024
Janes, K., & Kim, J.-H. 2009, in IAU Symp. 253, Transiting Planets, ed. F. Pont, D. Sasselov, & M. J. Holman (Cambridge: Cambridge Univ. Press), 548
Johns-Krull, C. M., McLane, J. N., Prato, L., et al. 2016, ApJ, 826, 206
Kamai, B. L., Vrba, F. J., Stauffer, J. R., & Stassun, K. G. 2014, AJ, 148, 30
Kipping, D. M. 2010, MNRAS, 407, 301
Kirk, B., Conroy, K., Prša, A., et al. 2016, AJ, 151, 68
Kolbl, R., Marcy, G. W., Isaacson, H., & Howard, A. W. 2015, AJ, 149, 18
Kovács, G., Zucker, S., & Mazeh, T. 2002, A&A, 391, 369
Kraus, A. L., Shkolnik, E. L., Allers, K. N., & Liu, M. C. 2014, AJ, 147, 146
Kurucz, R. L. 1992, in IAU Symp. 149, The Stellar Populations of Galaxies, ed. B. Barbuy & A. Renzini (Dordrecht: Kluwer), 225
Libralato, M., Nardiello, D., Bedin, L. R., et al. 2016, MNRAS, 463, 1780
Livingston, J. H., Dai, F., Hirano, T., et al. 2018a, AJ, 155, 115
Livingston, J. H., Dai, F., Hirano, T., et al. 2018b, arXiv:1809.01968
Lomb, N. R. 1976, Ap&SS, 39, 447
Lopez, E. D., & Fortney, J. J. 2013, ApJ, 776, 2
Lopez, E. D., & Rice, K. 2016, arXiv:1610.09390
López-Morales, M., & Ribas, I. 2005, ApJ, 631, 1120
Luhman, K. L., Mamajek, E. E., Allen, P. R., & Cruz, K. L. 2009, ApJ, 703, 399
Lundkvist, M. S., Kjeldsen, H., Albrecht, S., et al. 2016, NatCo, 7, 11201
Maíz Apellániz, J. 2006, AJ, 131, 1184
Mamajek, E. E. 2005, ApJ, 634, 1385
Mamajek, E. E., & Bell, C. P. M. 2014, MNRAS, 445, 2169
Mamajek, E. E., & Hillenbrand, L. A. 2008, ApJ, 687, 1264
Mandel, K., & Agol, E. 2002, ApJL, 580, L171
Mann, A. W., Feiden, G. A., Gaidos, E., Boyajian, T., & von Braun, K. 2015, ApJ, 804, 64
Mann, A. W., Gaidos, E., Mace, G. N., et al. 2016, ApJ, 818, 46
Mann, A. W., Gaidos, E., Vanderburg, A., et al. 2017a, AJ, 153, 64
Mann, A. W., Vanderburg, A., Rizzuto, A. C., et al. 2017b, arXiv:1709.10328
Martin, D. C., Fanson, J., Schiminovich, D., et al. 2005, ApJL, 619, L1
Masuda, K., & Winn, J. N. 2017, AJ, 153, 187
Meibom, S., Torres, G., Fressin, F., et al. 2013, Natur, 499, 55
Mentuch, E., Brandeker, A., van Kerkwijk, M. H., Jayawardhana, R., & Hauschildt, P. H. 2008, ApJ, 689, 1127
Mermilliod, J. C. 1981, A&A, 97, 235
Mermilliod, J. C. 2006, yCat, 2168, 0
Mermilliod, J.-C., Weis, E. W., Duquennoy, A., & Mayor, M. 1990, A&A, 235, 114
Meynet, G., Mermilliod, J.-C., & Maeder, A. 1993, A&AS, 98, 477
Morton, T. D. 2015, VESPA: False Positive Probabilities Calculator, Astrophysics Source Code Library, ascl:1503.011
Obermeier, C., Henning, T., Schlieder, J. E., et al. 2016, AJ, 152, 223
Owen, J. E., & Wu, Y. 2013, ApJ, 775, 105
Pace, G., Pasquini, L., & François, P. 2008, A&A, 489, 403
Parviainen, H. 2015, MNRAS, 450, 3233
Paunzen, E. 2015, A&A, 580, A23
Pecaut, M. J., & Mamajek, E. E. 2013, ApJS, 208, 9
Pecaut, M. J., & Mamajek, E. E. 2016, MNRAS, 461, 794
Pepper, J., Gillen, E., Parviainen, H., et al. 2017, AJ, 153, 177
Perryman, M. A. C., Brown, A. G. A., Lebreton, Y., et al. 1998, A&A, 331, 81
Petigura, E. A., Howard, A. W., Marcy, G. W., et al. 2017, AJ, 154, 107
Petigura, E. A., Marcy, G. W., Winn, J. N., et al. 2018, AJ, 155, 89
Petrie, R. M. 1958, MNRAS, 118, 80
Plavchan, P., Latham, D., Gaudi, S., et al. 2015, arXiv:1503.01770

Prosser, C. F. 1992, AJ, 103, 488
Quinn, S. N., White, R. J., Latham, D. W., et al. 2012, ApJL, 756, L33
Quinn, S. N., White, R. J., Latham, D. W., et al. 2014, ApJ, 787, 27
Randich, S., Pallavicini, R., Meola, G., Stauffer, J. R., & Balachandran, S. C. 2001, A&A, 372, 862
Rasmuson, N. H. 1921, MeLuS, 26, 3
Rebull, L. M., Stauffer, J. R., Bouvier, J., et al. 2016, AJ, 152, 113
Rebull, L. M., Stauffer, J. R., Hillenbrand, L. A., et al. 2017, ApJ, 839, 92
Rizzuto, A. C., Mann, A. W., Vanderburg, A., Kraus, A. L., & Covey, K. R. 2017, AJ, 154, 224
Rizzuto, A. C., Vanderburg, A., Mann, A. W., et al. 2018, arXiv:1808.07068
Rodriguez, D. R., Bessell, M. S., Zuckerman, B., & Kastner, J. H. 2011, ApJ, 727, 62
Rodriguez, D. R., Zuckerman, B., Kastner, J. H., et al. 2013, ApJ, 774, 101
Scargle, J. D. 1982, ApJ, 263, 835
Seager, S., & Mallén-Ornelas, G. 2003, ApJ, 585, 1038
Shkolnik, E. L., Liu, M. C., Reid, I. N., Dupuy, T., & Weinberger, A. J. 2011, ApJ, 727, 6
Shobbrook, R. R. 1983, MNRAS, 205, 1215
Skiff, B. A. 2014, yCat, 1020, 23
Soderblom, D. R., Hillenbrand, L. A., Jeffries, R. D., Mamajek, E. E., & Naylor, T. 2014, in Protostars and Planets VI, ed. H. Beuther et al. (Tucson, AZ: Univ. Arizona Press), 219
Soderblom, D. R., Jones, B. F., Balachandran, S., et al. 1993, AJ, 106, 1059
Stauffer, J. 1982, PASP, 94, 678
Stauffer, J., Rebull, L., Bouvier, J., et al. 2016, AJ, 152, 115
Stauffer, J. R., Barrado y Navascués, D., Bouvier, J., et al. 1999, ApJ, 527, 219
Stauffer, J. R., & Hartmann, L. W. 1987, ApJ, 318, 337
Stauffer, J. R., Hartmann, L. W., & Jones, B. F. 1989, ApJ, 346, 160
Tu, L., Johnstone, C. P., Güdel, M., & Lammer, H. 2015, A&A, 577, L3
Upgren, A. R., Weis, E. W., & Deluca, E. E. 1979, AJ, 84, 1586
van Leeuwen, F. 2007, A&A, 474, 653
van Saders, J. L., & Gaudi, B. S. 2011, ApJ, 729, 63
Vanderburg, A., & Johnson, J. A. 2014, PASP, 126, 948
Vanderburg, A., Latham, D. W., Buchhave, L. A., et al. 2016, ApJS, 222, 14
Vanderburg, A., Mann, A. W., Rizzuto, A., et al. 2018, AJ, 156, 46
Vazan, A., Ormel, C. W., & Dominik, C. 2017, arXiv:1712.06158
Ventura, P., Zeppieri, A., Mazzitelli, I., & D'Antona, F. 1998, A&A, 334, 953
Vogt, S. S., Allen, S. L., Bigelow, B. C., et al. 1994, Proc. SPIE, 2198, 362
Walter, F. M., & Boyd, W. T. 1991, ApJ, 370, 318
Walter, F. M., Brown, A., Mathieu, R. D., Myers, P. C., & Vrba, F. J. 1988, AJ, 96, 297
Weis, E. W. 1981, PASP, 93, 437
Weldrake, D. T. F., Sackett, P. D., & Bridges, T. J. 2008, ApJ, 674, 1117
Weldrake, D. T. F., Sackett, P. D., Bridges, T. J., & Freeman, K. C. 2005, ApJ, 620, 1043
Yee, S. W., Petigura, E. A., & von Braun, K. 2017, ApJ, 836, 77
Yu, L., Donati, J.-F., Hébrard, E. M., et al. 2017, MNRAS, 467, 1342
Yuan, H. B., Liu, X. W., & Xiang, M. S. 2013, MNRAS, 430, 2188
Zacharias, N., Finch, C., & Frouard, J. 2017, AJ, 153, 166